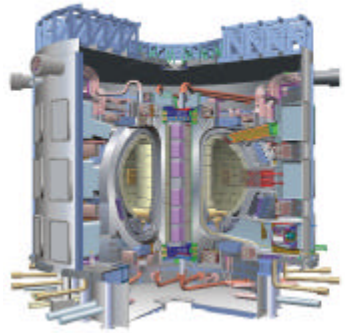

Education and Culture DG

Master of Science in Nuclear Fusion and Engineering Physics

Erasmus Mundus

Optical characterization of ion implanted silica.

Master Thesis
presented by

L. Alonso Araya-Solano

Thesis Promoters

Jose Ramon Martin Solis
Universidad Carlos III de Madrid

Guido van Oost
Universiteit Gent

July 8th, 2012

UNIVERSITEIT GENT

UNIVERSIDAD COMPLUTENSE MADRID

Universidad Carlos III de Madrid

Universität Stuttgart

UNIVERSITÉ DE LORRAINE

KTH VETENSKAP OCH KONST

Optical characterization of ion implanted silica.

Master Thesis
presented by

L. Alonso Araya-Solano

Thesis Promoters

Jose Ramon Martin Solis
Universidad Carlos III de Madrid

Guido van Oost
Universiteit Gent

Thesis Supervisor
Piedad Martin

Erasmus Mundus Program on Nuclear Fusion Science and Engineering Physics

July 8th, 2012.

Abstract.

Amorphous silica is a candidate material for the majority of optical systems in fusion technology because of its high transparency. Radiation can modify the optical properties of the diagnostic systems materials used in fusion, so the understanding of the optical characteristics of silica under radiation is of great interest. Ion implantation is widely used as a means of introducing radiation damage in materials.

Optical characterization of three silica types implanted with Si and O ions at different fluences has been done. One of the silica is the commercially available infrasil I301 and the other two are reference materials in the ITER context: KU1 and KS4V. During the implantation the ionoluminescence spectrum was obtained (between 1.5 and 6 eV) to study the evolution of different defects with implantation fluence. Once implanted, the optical absorption spectrum of the samples was measured from vacuum ultraviolet to near infrared (8.2 to 0.4 eV).

Three main bands for the ionoluminescence spectra of all silica types were found: one band at 2.7 eV associated to self-trapped excitons (STE) defects plus oxygen deficient defects (ODC II). Another band at 1.9 eV associated to non-bridging oxygen hole centers (NBOHC). And finally a band at 2.3 eV corresponding also to STE defects.

The absorbance of all silica types presented five perfectly differentiated bands corresponding to ODC II (5 eV), dangling silicon bond E' (5.8 eV), NBOHC (6.7 and 7.4 eV) and neutral oxygen vacancy ODC I (7.7 eV).

Contents

Chapter 1.

Introduction.

Many diagnostic systems in the ITER need materials to be directly exposed to radiation. Therefore it is necessary to keep intact the mechanical and physical properties of these materials under radiation. In optical diagnostic windows, lenses, mirrors and optical fibers will need to transmit signals over a broad spectrum, including ultraviolet, visible and infrared wavelengths (Ref. [1]).

Amorphous silicon dioxide (or silica) is an important material widely used in different technology fields like optics and electronics and in nuclear and spatial related applications. It has one of the highest transparencies of all materials in the ultraviolet and vacuum ultraviolet range, which makes it perfect for low loss in optical components as optical communication fibers and windows (Ref. [2]). The mechanical and chemical characteristics of the silica make it ideal against radiation environments, although its optical and electrical properties are strongly influence by defects, which are introduced during the manufacturing process or are produced by photon radiation (UV light, X rays or ? rays) or particle radiation (ions, electrons or neutrons) (Ref. [3]). The optical degradation (radiation induced optical absorption and light emission) impose severe limitations on the use of any optical material within a radiation field. Then, the understanding of the intrinsic defects of the silica structure and the radiation consequences on it has a mayor importance.

Ion implantation is widely used as a relatively low-cost and rapid means of introducing radiation damage in materials. Implantation can be carried out in vacuum and at well controlled temperatures. Self ion implantation (of the same atomic species as constituent) is used to introduce displacement damage. Implantation with particle accelerators have disadvantage (with respect reactor irradiations) because of the limited irradiation volume and particle penetration depth.

It is the particular interest of this work to study the effects of silicon and oxygen implantation on the optical properties (as absorption and luminescence) of different silica types.

The samples used in this work were high purity fused silica with different OH content: KU1 (high OH, about 820 ppm) and KS4V (low OH, <1ppm), which are known for being highly radiation resistant and considered as reference materials in optical components of fusion devices (ITER). And also a commercial silica with higher metallic impurity content; infrasil 301. The irradiations were performed with O^{+4} ions (with energy of approx. 13.5 MeV) and Si^{+4} ions (with energy of approx. 24.3 MeV) at several fluences to study this radiation effect and correlate it to defects creation.

The ionoluminescence (IL) spectrum was measured during ion irradiation in order to analyse the evolution of different defects. After ion implantation the samples were characterized by optical absorption measurements. The spectra were measured in a wide wavelength range from VUV to NIR.

Chapter 2.

Amorphous Silicon dioxide.

2.1 Structure and types.

SiO_2 can have crystalline form (as quartz, cristobalite, coesite, keatite, stishovite, chalcedon, agate, moganite and others) or amorphous form (as opal, hyalite, sintered pearl, lechateierite and natural silica glass). The structural unit of SiO2 is the tetrahedron, as is seen in figure 2a. This SiO_2 unit cell is composed of 4 oxygen atoms, each one located at the vertices of the regular tetrahedron. A single silicon atom is located in the inner center of the tetrahedron. The silicon atom has four hybridized sp^3 orbitals, therefore it has four electrons in the outermost energy shell. An oxygen atom has two valence electrons (two electrons in the outermost shell), then a silicon atom can take four oxygen atoms and form a stable bond (Ref. [4]). This results into the SiO2 molecule. The electron remaining from each of the oxygen linked to the central silicon atom can be also linked to another silicon atom and thus, construct another tetrahedron. The arrangement of the links between tetrahedron units determines the classification of the silicate. If the tetrahedrons exist isolated the material is called nesosilicate, if they are linked in group of two they are called soroslicate, if all tetrahedrons are linked together into rings the material is called cyclosilicate (Ref. [5]).

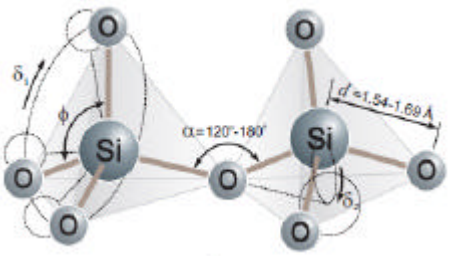

Figure 2a. The basic structure of the SiO2. *d* is the Si-O bond length. a is the inter-tetrahedral angle. F is the tetrahedral angle, and the d's are the bond torsion angles (Ref. [6]).

The Si-O bond length can vary in the range of 0.154 nm to 0.169 nm. While the angle a varies as the silica form changes. For example for vitreous silica varies from 120 to 180 and for quartz varies from 146 to 155° (Ref. [6]). The different arrangements of the tetrahedral units produce the different types of silicate structure.

The amorphous silica or vitreous silica can be divided into several types according to its method of fabrication and its OH (hydroxyl group) content. Here the amorphous silica is referred simply as silica. Often the silica is divided into four types (Ref. [7]).

- The *type I* (natural dry) is molten quartz (silica obtained from ground quartz or quartz sand) with low OH content. It is obtained by melting quartz sand or quartz powder by electric fusion. The aluminium is the

predominant impurity in natural quartz, and it keeps its presence in the final product making the type I silica high in aluminium impurities.

- *Type II* (natural wet) silica is molten quartz with high content of OH. It is obtained by melting quartz powder. This powder is melt in a H2/O2 flame giving rise to a high content of the OH molecule in the resulting silica.
- *The type III* (synthetic wet) is synthetic silica produced by the oxidation and hydrolysis of the SiCl4 in a H2/O2 flame. In the process of production this silica is able to absorb great quantities of water from the atmosphere. As consequence the type III silica has high content of OH group, even more than type II. Also it has considerable content of chlorine due to the initial reactants.
- The *type IV* (synthetic dry) is silica obtained from the oxidation of SiCl4. The difference of this silica type with respect the latter is that a chlorination treatment is applied at high temperatures, reducing the content of OH (Ref. [8]).
- Finally the *type V* is a special type of silica (like the KS4V) produced by a complex process which involves gasification of silicon (from polysilicic acid), oxidation of the gas to form silicon dioxide and thermal fusion of the resulting molecule in vacuum.

2.2 Main optical defects.

The next is a brief review of the points defects in amorphous or glassy silica. Vacancy-interstitial defects (the so called Frenkel defects) present in glass and quartz are similar. The most of the defects observed in the bulk silica are also observed on the surface, including the silicon and oxygen dangling bonds centers. Sometimes the defects are divided into Frenkel defects (ODC I and POL) and dangling bonds defects (the rest). Defects due to impurities are called extrinsic defects.

E' center or silicon dangling bond center.

The generic E' center comprises an unpaired electron in a dangling tetrahedral (sp3 hybridized) orbital of the silicon atom which is bonded to three oxygens in the silica network; $\equiv Si\bullet$. The lines represent the three oxygen bond to the silicon atom and the dot an unpaired electron. This center gives a narrow characteristic EPR (electron paramagnetic resonance) signal (Ref. [9]). The second neighbour environment of the bulk types of E` centers remain under discussion. It is associated with an absorption band at 5.85 eV in quarts and silica glass.

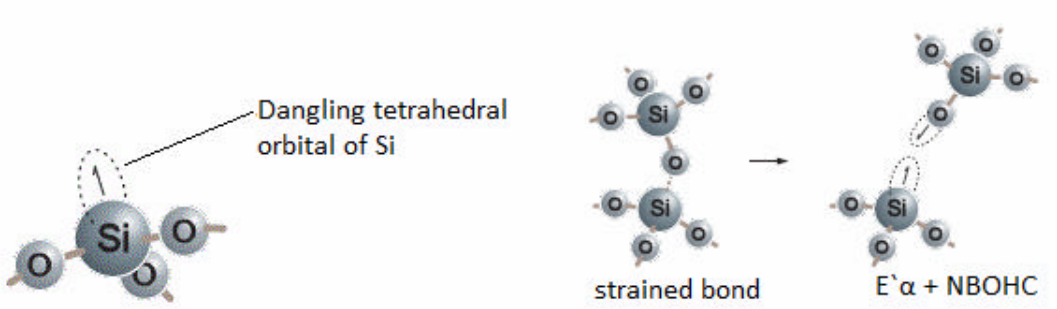

Figure 2b. The E` center and a creation process of E'_{α}. Ref. [6].

There are four main types of the E' center defects in vitreous silica, labelled with their corresponding spectroscopic notation as E'_{α}, E'_{β}, E'_{γ}, E'_{s}. One of the mechanism that may produce the E`a defect is the rupture of the strained bond (=Si-O- Si=) producing the E'a plus one NBOHC defect.

The absorption of a hydrogen atom by an unrelaxed oxygen vacancy configuration may lead to the formation of a E'_{β}. The rupture of an unrelaxed oxygen vacancy configuration also can lead also to the E'_{γ} defect.

The electron paramagnetic resonance (EPR) signal of the E`? (the most abundant type) is related to a strong absortion at 5.8 eV. The dangling Si bond on surface has an absorption band at 6.2 eV. If one of the neighbouring O in the silica molecule is substituted by one H an optical band appears at 4.9 eV (Ref. [2]).

Oxygen deficient centers (ODC).

There are two ODC kinds. The ODC I is a simple oxygen vacancy. It is also known as oxygen deficient vacancy. It is denoted as =Si-Si=, where the single – represent the two bonded electrons in a chemical reaction. It's the only optical absorption band that is observed on both silica glass and in alpha quartz (type of silica crystal).The absorption band attributed to ODC I is at 7.6 eV. The ODC I can also be transformed into =Si-H through a thermal reaction with hydrogen. This defect is precursor of the E'centers (Ref. [10]).

The origin of the ODC II is still a matter of controversy. Two dangling bonds in Si can react forming a Si-Si bond or creating a divalent Si atom =Si•• (ODC II). These processes occur in the bulk of the silica. Its main difference with respect to the ODC I is the unrelaxed state of the oxygen vacancy. The absorption band associated to ODC II is about 5 eV. Two photoluminescence bands at 4.4 eV (singlet state to singlet state transition) and 2.7 eV (triplet state to singlet state transition) are related to the excitation of the bands 5 and 7.6 eV, evidencing the interaction of the ODC I and ODC II. Both ODC's are diamagnetic defects (non-paramagnetic), which means that they are not detectable by techniques as EPR (Ref. [11]).

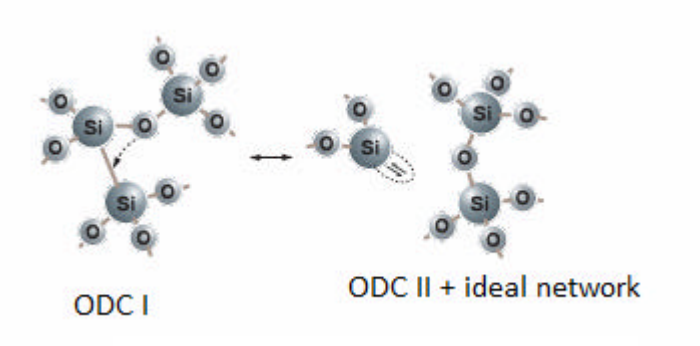

Figure 2c. ODC II from ODC I. Ref. [6].

The non bridging oxygen hole center (NBOHC).
It's an oxygen dangling bond defect (≡Si- O•). It is a paramagnetic defect and it is not present in alpha quartz, for they are not containing amorphous regions. It can be characterized by EPR and OA. It has an absorption band at 4.8 eV with FWHM of 1.07 eV. Also has a weaker asymmetric absorption band at 1.97 eV, FWHM 0.17 eV. A photoluminescence band at 1.91 eV appears with the excitation of its main absorption bands. This luminescence is on the red interval of the visible spectra. There is a third absortion band at 6.8 eV, confirmed by finding an excitation band at 6.4 eV for the 1,9 eV photoluminescence band of NBHOC (Ref. [2]).

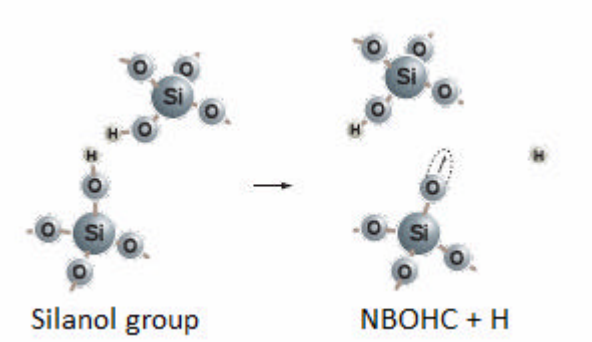

Figure 2d. One way of creating NBOHC. Ref. [6].

NBHOC are created when hydrogen atoms are liberated radiolytically (disassociated by nuclear radiation) from a hydroxyl radical OH in high OH group silica (wet silica), that is, they are created by the rupture of silanol groups (≡Si-O- H). Although the NBOHC can also be created in low OH group silica (dry silica) by the rupture of the strained Si-O bond.

Peroxy bridge or interstitial oxygen (POL).
It is an oxygen excess in between Si-O bond (≡Si-O-O-Si≡). It is a diamagnetic defect. The peroxy bridge plus hydrogen atoms is a precursor of the silanol bonds. Also the peroxy bridge is precursor for peroxy radicals. The POL absorption band is about 6.4-6.8 eV, which is hard to be detected because of the background of other bands in that spectra interval and its small oscillator strength. Photolysis (molecule broken by photons) of interstitial O_2 causes strong bleaching (decrease in the optical absorption) of the associated wide optical absorption creating absorption at 7.1 eV (Ref. [12]).

The peroxy radical (POR).

It is a paramagnetic defect with a hole delocalized in an antibonding (p type) orbital in a O-O bond. Represented by ≡Si-O- O•. Figure V shows some possible generation of the POR. It is created via adding to an interstitials O to a oxygen dangling bond. Its optical properties are unknown, however according to some experimental evidence it has been suggested that its absorption band is about 7.7 eV. It has a well known surface absorption band at 5.4 eV (Ref. [6]). Pseudobands are created by the closeness of POR and NBHOC.

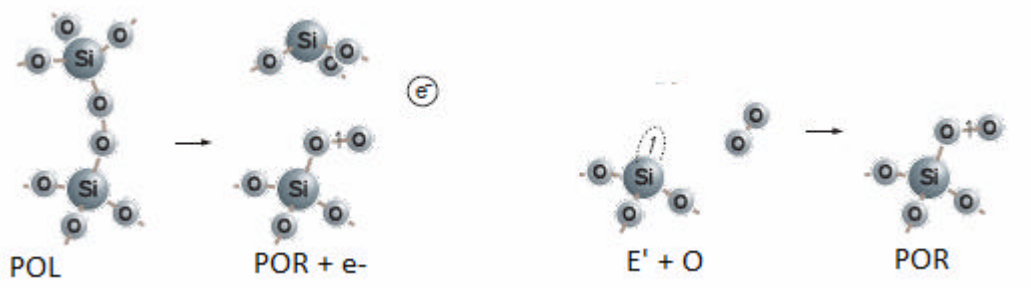

Figure 2e. Creation of peroxy radical defect. Ref. [6].

The self-trapped exciton (STE).

The exciton is a neutral quasi particle that consists in a bound state of an electron and a hole which are attracted to each other by coulomb forces. The STE is defect related to the excitation energy in electron and holes interaction. Selftrapping occurs in an otherwise ideal structure when the excited electron and hole spontaneously create a localized distortion in the lattice which lowers their total energy and thus localizes and traps them at the distortion (Ref. [13]). Luminescence band in the range of 2 to 3 eV are considered to belong to the STE. The characteristic blue light in amorphous SiO_2 is attributed to the STE. The decay of a STE associated to an excited Si-O bond can create an oxygen vacancy and peroxy bridge. Also creating STE's in silica leads directly to the formation of two other important defects, the E' center and the NBOHC (Ref. [13]).

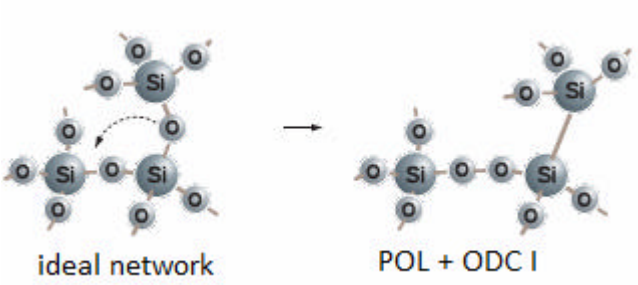

Figure 2f. Decay of STE due to an excited Si-O bond creating a peroxy bridge and a oxygen vacancy. Ref. [6].

Others.

Hydroxyl groups (OH) are one of the main impurities in silica (that is the reason why they are used to characterize silica types). OH can be precursors of E' and NBOHC. Reaction with water molecules is the main source of OH groups (Refs. [14,15]). Molecular hydrogen can also generate hydroxyl groups (Ref. [16]). Silanol groups (≡Si-OH) are a hydroxyl groups bonded to silicon atoms (Ref. [17]).

2.3 Optical absorption and ionoluminescense.

The optical absorption is related to the interaction between electromagnetic radiation and matter. Optical absorption is produced if the energy of any incident radiation on certain material is higher than the difference between the energy associated to the valence band (bonded electrons with no mobility) and the energy associated to the conduction band (free electrons) of the material; but also for the OA to happen the beam frequency have to be resonant with ground to excited state transition of the atom in the solid. If the energy is inferior to this absorption limit, then the material is "transparent". If the radiation energy is superior to the absorption limit the resultant absorption spectrum could be continuous. The defects in an insulator (as silica) can produce new energetic levels between the conduction band and the valence band (band gap). Therefore new internal energetic transitions can appear producing new absorption or luminescence bands for the material as consequence of its defects. The absorption energy and its associated energy width could characterise the defects. Furthermore the intensity of one particular absorption band in an absorbance spectrum is proportional to the number of related defects (Ref. [18]).

Point defects are immersed within the material surrounded by atoms. These atoms vibrate around their equilibrium position affecting the electronic states of the defects. Analogously, in a reciprocal dynamics the defects can affect the equilibrium position of the atoms around them. This interaction between the network vibration and the electronic states is known as phonon-electron coupling. The Huang-Rhys factor is a measure of the strength of the electron-phonon coupling.

Assuming defects with only two associated electronic states, these two states can be described as quantum harmonic oscillators. If over the system strikes electromagnetic radiation with energy equal to the energy difference between two electronic states, the system will absorb the incident energy and then electronic transition between the initial and final states take place. At T=0 a purely electronic transition (no phonons involved) can happen (the zero phonon line). At high temperatures when the electron phonon coupling is strong the zero phonon line is weak compared to the phonon sidebands. As the time associated to this transition is shorter than the vibration time related to the nucleus; the nucleus does not vary their position. Once the electronic transition happened the system relaxes until it reaches its minimum energy configuration by a emission of a phonon. This relaxation implies a phonon state change in a non radiative process. Then the system can go back to the initial state by a photon emission (for example after being irradiated with ions, like in the *ionoluminescence* process) where it can change its modes of vibration (phonon) again looking for the minimal energy configuration (Ref. [20]). As consequence the photon emission has a lower energy (lower frequency) than the absorption energy. This is known as Stokes displacement. The absorption process can occur between different states among the initial and the final states. The number exited states will decay exponentially with time according their mean life time (time necessary for the number of states decrease a factor of *e* its initial value) (Ref. [21]).

The intensity of any incident electromagnetic radiation diminishes as consequence of the energy absorption by the material, this attenuation is given by:

$$I(x) = I_0 e^{-\alpha x} \tag{4.1}$$

where a is the absorption coefficient, x the penetration deepness and I_0 the incident intensity (Ref. [18]). In the quantum mechanics view the intensity of electronic transition between two states is proportional to the square of the overlap integral of the excited and ground state. In the absorption process, the energy loss by the electromagnetic field for a length dl of material having N absorbers per volume unit is proportional to (Ref. [22]):

$$-dI(E) \propto I(E) N d(E - \Delta E) \left| \langle j_1 | er | j_0 \rangle \right|^2 dl \tag{4.2}$$

where $I(E)$ is the intensity of the incident light, $?E$ is the energy difference between the two transition states, and $f_0/er/f_0$ is the transition rate between the ground f_0 state and the excited state f_0 (Ref. [3]).

The absorbance or optical density is defined as the logarithmic ratio between the radiation passing thought a material and the reference intensity of the radiation before it passes the material:

$$OD = \log(I_0 / I) \tag{4.3}$$

This latter equation was used in the obtaining of the absorbance of the silica samples. The OD is dimensionless (Ref.[18]). The absorbance spectrum can be adjusted as a sum of Gaussian peaks, these peaks allow the identification of the defects structure. Each Gaussian peak is a normal Gaussian distribution, often used as first approximation to described random valued variables that go around a mean value, as the following equation:

$$G = \frac{1}{s\sqrt{2p}} e^{\frac{-}{2}\left(\frac{x-c}{s}\right)^2} \tag{4.4}$$

where c is the mean or expectation value (position of the peak); and s is the width or standard deviation. The full width at half maximum (FWHM) is defined as the width of a normal distribution at a level that is just half of the maximum of an ordinate peak. The relation between the FWHM and s is defined in the following equation:

$$FWHM = 2\sqrt{2\ln 2}s \tag{4.5}$$

The shape and the Full Width at Half Maximum (FWHM) of the peaks and bands in the luminescence spectrum depend on thermal effects (e.g. energy distribution of free charge carriers) and the strength of the interaction between the electrons and phonons, which participate in the optical transition. Assuming low temperatures and weak electron-phonon-interactions the luminescence spectra consist of sharp peaks and narrow bands. Strong electron-phonon-interactions yield to a broadening of the peaks and bands in the spectra.

The luminescence induced by ion beam irradiation is called *ionolumenescence* (IL). IL is an appropriate technique to investigate the microscopic processes accompanying the generation of damage, its kinetic evolution with the irradiation fluence and the formation of light centers (Ref. [23]). IL consists in analyzing the light emission induced by ion bombardment of a target material, which provides information about the intrinsic properties of medium network. The IL results from

the activation of radiative centers, whose excitation comes from the ionization of the sample layer crossed by the impinging ions (Ref. [24]).

The interactions between the ions penetrating the sample and the sample atoms lead to energy deposition within the sample. The generation of luminescence can be explained by the following processes:

- Ionization of sample atoms due to the energy deposition in the sample.
- Recombination of electrons and ionized atoms:
  a. the lattice absorbs the released ionization energy.
  b. excitation of the "optical system".
- De-excitation due to radiationless recombinations of excited states.
- Luminescence due to recombinations of excited states.

Defect centers (e.g. imperfections in the crytal lattice, impurities) can locally modify the electronic structure of the solid, yielding to the presence of *localized excited states* (e.g. creation of energy levels in the band gap of semiconductor materials by doping). The transitions resulting in intrinsic luminescence can be; (i) Recombination of free electrons in the conduction band with holes in the valence band (direct and indirect transition), (ii) Recombination of excitons (electrons and holes are bound by Coulomb-interaction, thus forming electron-hole-pairs), (iii) Electron Transitions from excited states of a defect center to its ground state.

During implantation, ions transfer energy to the target at rates of the order of keV per μm of path length by a mixture of electronic excitation and nuclear collisions. Below around 500 keV nuclear collisions lead to displacement of lattice ions and, via secondary collisions, cascades of displacements (Ref. [25]). The stopping power plays a major role in the understanding of the implantation. Theoretical estimates of the stopping require accurate knowledge of the interaction potential between the ion and target atom. Electronic stopping is proportional to ion velocity for lower-energy implants. At higher energies (>MeV) the electronic stopping cross section falls and the target becomes more transparent to the ions (Ref. [25]). Nuclear collision produce atomic displacements as in the curse of 10^{-14} s some hundreds of keV are deposited along the ion track. Typical displacement energies of lattice atoms range from 10 to 40 eV. The cascades of damage involve many atoms, and it depends among other things on the ion energy and cross section of the target material. The majority of atoms related to a cascade will relax back onto normal lattice sites although numerous vacancy features remain within the core of the cascade and interstitials are moved away from the ion track (Ref. [26]).

Radiation damage can be divided into several components, which are: displacement damage, ionization effects and transmutation (Ref. [1]). Displacements are due to knock on collision, displacing atoms or ions for their lattice sites giving raise to vacancies and interstitials (Ref. [27]). Once the atom is displaced its final position will be determined by the atoms mobility, which highly depends and is proportional to the temperature. The unity of measure of the displacement damage is the displacement per atom (dpa). This quantity measures the number of times in average that each atom is displaced from its site. The ionizing radiation is responsible for strengthen the dynamics of the grain boundaries on the surface of the material. Also the effects of the ionizing radiation are the excitation of electrons from the valence band to the conduction band, producing charge transfer effects in the material. The polyatomic nature of insulators and silica makes difficult the analysis of the response of them to both

displacement and ionizing radiation. Displacement damage can be caused in some cases by radiolysis (ionization alone). Finally, high energy radiation can produce nuclear reactions resulting in transmutation products which can modify the properties of the material and even giving rise to radioactive products.

For the optical properties of insulators the existing defects may change charge state under radiation and form colour centers and also new defects will form because of electronic excitation (Ref. [28]).

Techniques as cathodoluminescense (CL) and photoluminescense (PL) find good agreement with the IL technique in the identification of defects (Ref. [29]).

Some advantages of ion implantation are: The ion beam is monitored as a current, so precise control of the number of implanted ions is simple. (ii) The depth of the implant is controlled by the ion energy and hence a judicious choice of energy and dose can develop any desired impurity profile beneath the surface. (iii) Different ions may be placed at different depths. (iv) Implants may be made at any target temperature so one can use impurity doping in low-temperature crystal phases (Ref. [25]).

Chapter 3.

Implantation process simulation using SRIM.

Previously to the implantation of the silica samples the program SRIM (Stopping and Range of Ions in Matter) was used. With this program is possible to make simulations of the implantation process in silica and thus obtain the average penetration depth of the ion beam in the sample. So this program allows to set the necessary parameters in order to get a similar penetration in the samples implanted with O ions and Si ions. The plots on this section are from SRIM.

The approximation was made by setting silica quartz as target with a density of 2.21 g/cm^3 (the amorphous silica density). The displacement energy (the necessary energy to displace one oxygen atom out of its lattice) for the oxygen atoms was set as 20 eV and for silicon atoms was set as 35 eV (Refs. [30,31]). The ion energies used were 24.3 MeV for Si ions and 13.5 MeV for O ions.

SRIM calculates the number of vacancies created by ions of the implantation beam and vacancies created by recoils atoms which may cause recoils cascades as well. For the high implantation energies considered here the penetration length of one ion is hundred times larger than the scale of movement of one single recoil atom (not considering the entire length of the movement of recoils atoms participating in a cascade effect).

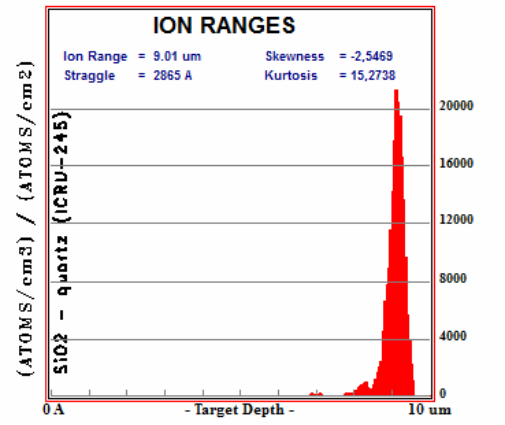

Figure 3a. Ion distribution for Si implantation.

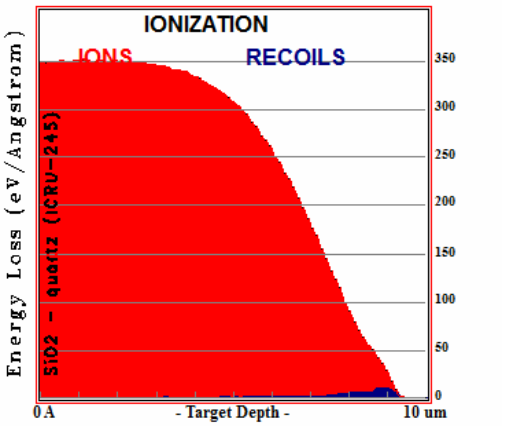

Figure 3b. Energy loss for Si implantation.

On figure 3a kurtosis is a measure of the "peakedness" of the distribution and skewness is a measure of the asymmetry of the silicon ion distribution. The highest intensity for silicon ion penetration is at 9.01 µm. At this depth the impurity concentration is about 1.6×10^{19} atoms/cm3 (20000 a/cm × 8×10^{14} ions/cm^2~ 1.6×10^{19} atoms/cm3) considering a flow of 2.5×10^{11} ions/cm^2 s (the implantation flow) after more or less 50 minutes of irradiation (2.5×10^{11} ions/cm^2

s × 50 min~8×10^{14} ions/cm^2; this is one of the typical fluencies that was used our experiments).

As can be seen in figure 3b the most of the energy loss caused electronic excitation (ions), just a small part of the deposited energy was lost into producing recoils.

Any knock off of a lattice atom of its site is considered a displacement (Ref. [32]). The displacement produced on the sample is equal to the vacancies produced by the ions of the incident beam or any recoil atom plus the replacement collisions (atoms site with new atoms identical to their original atom, this definition also includes the replacements with ions of the incident beam). Figure 4c shows the displacement distribution.

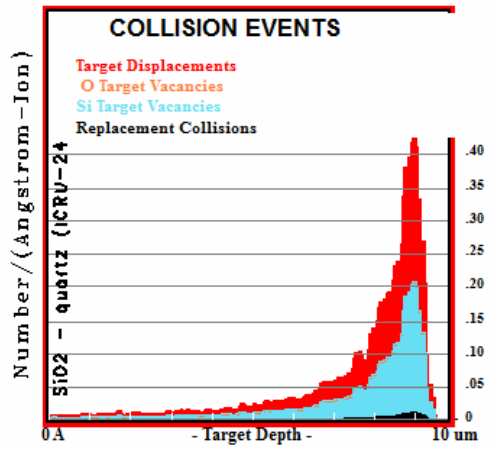

Figure 3c. Collision events for Si implantation.

The plot 3c gives an approximate maximum of 0.35 vacancies/(A-ion) at 9.02 µm. The following is an illustrative example related to the damage produced in the sample: after a rough calculation and considering that the damage anneals instantly up to 99% (so 1% is left as permanent damage) and also considering a fluence of 8e14 ion/cm^2, which is the approximated result of a flow of $2.5\text{x}10^{11}$ ions/cm^2 s in 50 minutes; the final damage would be about 5% of the whole sample volume.

In the case of the oxygen implantation the most of the ions reached a depth of 9.04 µm. Figure 4d shows the distribution for the oxygen implanted ions. According to the SRIM simulation the implantation depth over silica for silicon ions of 24.3 Mev and oxygen ions of 13.5 MeV is very similar. Also is remarkable from the ionization plots that the stopping power at the sample surface for Si ions is about 3.5 KeV/nm while the stopping power for O ions is around 1.6 KeV/nm.

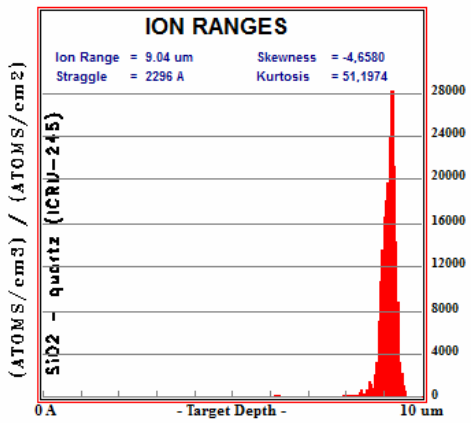

Figure 3d. Ion distribution for O implantation.

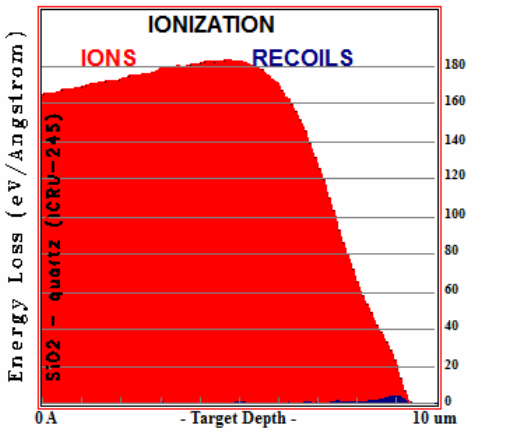

Figure 3e. Energy loss for O implantation.

On figure 3f, replacement collisions events are more or less the same compared to the Si implanted case, although one may think there should be more because of the more availability of places for O in the SiO_2 molecule.

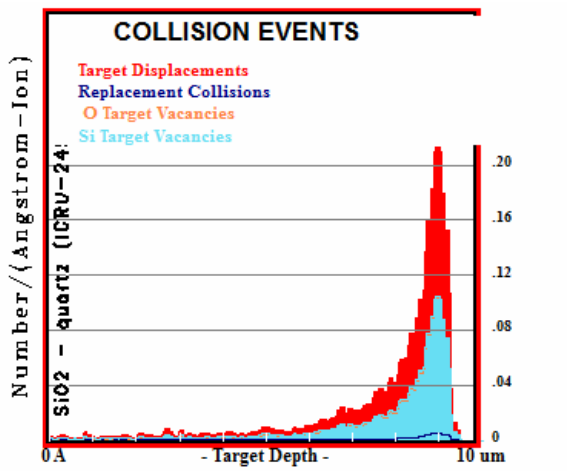

Figure 3f. Collision events for O implantation.

Chapter 4.

Experimental.

Types of silica used in the present work.
Three silica types were used: I301, KU1 and KS4V. The infrasil (I301) is a type I silica. It is produced by the commercial company Heraeus. The KU1 (type III) is a high purity silica with high content OH groups, while the KS4V (type V) is also a high purity silica but with much lower content of OH. These latter two silicas were provided by the Russian Federation to CIEMAT (Research Center of Energy, Ambient and Technology, Spain) in the ITER framework collaboration. These three silica types are reference materials in the ITER context mainly because if their high endurance against radiation (Ref [33]). The table A gives approximated contents of the impurities of the different amorphous silica types used in this work.

Name	Silica type	OH (ppm)	Al (ppm)	Cl (ppm)	Trace impurities (ppm)
I301	I	= 8	20	undefined	=6
KU1	III	~ 1000	1.4	100	= 2.7
KS4V	V	= 0.1	< 0.08	<1	= 0.1

Table A. Contents of the silica types utilized in this work (Refs. [8, 33, 34]). The trace impurities include Ca, Na, Fe, Cr, K, Li, Mg, Ge and Ti.

4.1 Implantation process and Ionoluminescence spectra measurements.

The silica samples were implanted at the CMAM (Materials Micro-Analysis Center from Universidad Autónoma de Madrid). The surface size of the samples was about 10x10 mm and 1 mm thickness. Samples were irradiated in a standard scattering chamber at a vacuum of 10^{-4} Pa using a 5 MV Tandem accelerator. The size of the ion beam was of 5x5 mm. Fluences were determined by direct current integration on the target using electron suppression. The current was 45 nA, obtained with a faraday cup (cup designed to catch charged particles).

During the implantation the ion-luminescence emission of the sample was transmitted through a silica window placed at 45 degrees with respect to the ion beam and then collected and focused via a lens into a silica optical fiber, figure 4.1. The light was guided to a spectrometer (type QE6500) configured with a CCD (charge coupled device) array detector (where electrons generated are proportional to the energy of the incident photon). In this spectrometer the whole spectrum was measured simultaneously, with an integration time of 3 seconds or 5

seconds; that is each 3 or 5 seconds a total spectrum is collected. The spectrum collected in this part goes from 200 to 800 nm (around 1.5 to 6.2 eV).

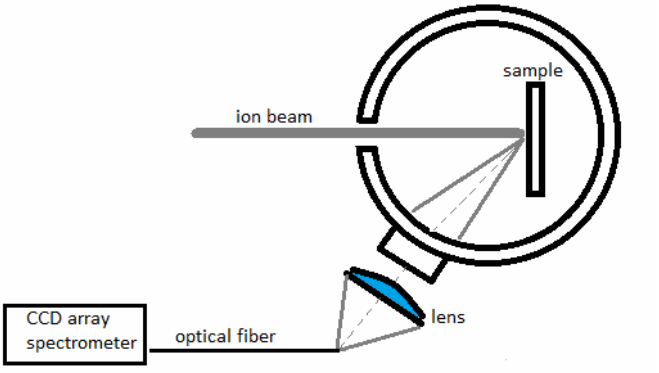

Figure 4.1. Schematic of the IL measurements.

Due to the high sensitivity of the IL with small current fluctuations (around 1 nA), it was necessary to record the real time evolution of the current to discriminate variation of the IL, either caused by the kinetics of the damage or those associated with current changes (Ref. [23]).

4.2 Optical absorption measurements in the VUV and UV-vis range.

I. After implantation the optical absorption spectra of the implanted samples was measured. In the ultra violet (UV), visible (VIS) and near infrared (NIR) range a Varian spectrometer (double beam spectrometer) model Cary 5E was used. The range measured is in between 3000 nm to 190 nm wavelength. The basic operation of this device is presented in figure 4.2. Two lamps, one of tungsten (for visible and near infrared range) and one of deuterium (for ultraviolet spectrum) are utilized as the source of light. The light given by the source pass through a monochromator, which selects a narrower interval of the polychromatic spectrum. Then this monochromatic beam is divided into two beams by means of an optical rotating wheel. One beam pass through a sample and the other beam is used as reference. The two beams reach a photomultiplier detector. Then the optical absorption spectrum of the sample is compared with the reference spectrum, and so the final absorption spectrum is independent of the intensity of the light source. The schematic of this system is presented in figure 4.2.

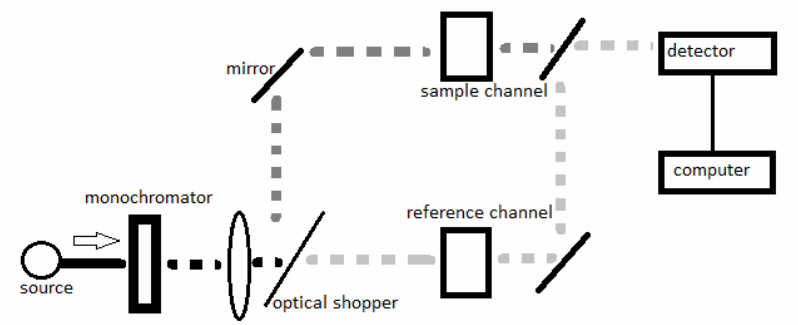

Figure 4.2. Double beam spectrometer.

II. The absorption spectra for the vacuum ultraviolet range were measured in a composed system illustrated in the figure 4.3. A McPherson deuterium lamp model 632 was used as light source. The emission of this lamp goes from 380 to 110 nm. A Seya-Namioka monochromator (Mcpherson 234/302, focal length 200 mm) is coupled to this lamp, which uses an aberration concave grating (of 1200 g/mm) to obtain optimal performance. The detector was a photomultiplier (Electron Tubes 9405B) with magnesium fluoride window, rubidium telluride photocathode and eleven BeCu dynodes of linear focused design. One of the more important characteristics of this detector is that does not respond to visible light (solar blind). Its spectral response goes from 110 to 300 nm. The vacuum in the detector had to be set lower than 10^{-4} Torr to avoid malfunction. The samples were placed into a rotating holder. The current in the detector was measured with a picoamperimeter (Keithley 6485) and then together with the monochromator scan control (McPherson 789A-3) the optical absorption was obtained. To obtain the OD we have compared the system response to the emission of the deuterium lamp (spectrum without sample) and the response emission through the sample (single beam spectrometer model).

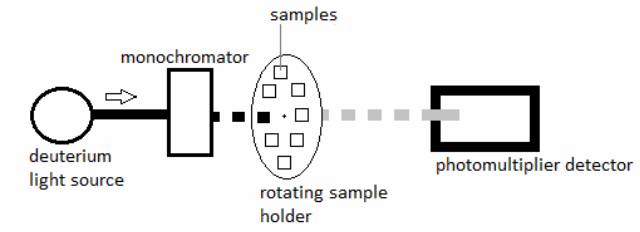

Figure 4.3. Single beam spectrometer.

Chapter 5.

Results.

5.1 Ionoluminescence results.

With the SRIM program a simulation of the ion implantation was carried out. The energies selected were 13.5 MeV for the oxygen ions implantation and 24.3 MeV for the silicon ion implantation. The irradiations with these ions were performed with several fluences in order to study their effect and correlate defect creation with local non stoichiometry (undefined proportions in compounds) in the silica samples.

It is important to consider that the time at which the spectra were recorded corresponds to a certain fluence received by the sample. The implantation flow was about 2×10^{11} ions/cm^2 s, and then the corresponding approximated fluences are:

10s? 2×10^{12} ions/cm^2
15s? 3×10^{12} ions/cm^2
50s? 1×10^{13} ions/cm^2
300s? 6×10^{13} ions/cm^2
2500s? 4×10^{14} ions/cm^2

5.1.1 Ionoluminescence during Si implantation in I301, KS4V and KU1.

Silicon implanted I301.

The spectrum shown in figure 5.1a presents a typical ionoluminescense (IL) spectrum. The two main peaks at 1.9 and 2.7 eV observed in figure 5.1a corresponds (according to Jimenez et al.) to a NBOHC center (Ref. [24]) and to emission from a self trapped exciton (STE) in the SiO2 network respectively (Refs. [23,36]). Furthermore the luminescence in the 2.7 eV band is also attributed to ODC II centers (Ref. [35,24]). For the first collected ionoluminescence spectra at 15 s there is a little difference presented as a “tale” on the right of the larger band at 2.7 eV approx. This small band may be due to defects in the silica network induced by impurities as Ge (Ref. [37]) and disappear with implantation fluence. Also minor bands from Fe impurities at 1.65 eV and radiative recombination of the self trapped exciton with an E` center (at 2.26 eV) are present in the spectrum [19]. These basic peaks of the ion luminescence spectrum are presented in figure 5.1b over the 10 s (II) and 50 s (I) curves, in which a Gaussian function was used to fit them. From figure 5.1a it is clear that there is maximum in the 2,7 eV band at about 50 seconds. Thus as the time passes the IL yield grows till the 50 seconds, and then the yield starts decreasing becoming even less intense that the one at 15 s. Over 200 s of the fluence the spectrum is practically constant with time, that is, the ionoluminescence spectrum appears to

be saturated after this time. The decrease in the luminescence intensity after its maximum could be explained because of the formation of clusters from ODC defects, this is, groups of ODC interacting together to inhibit the yield at 2.7 eV (Ref. [23]) and also because recombination of defects.

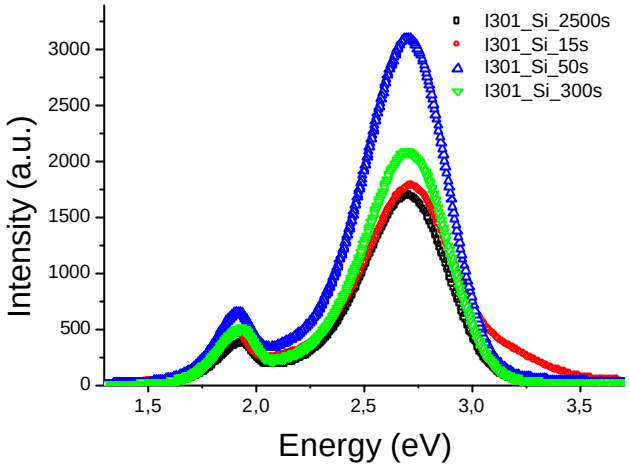

Figure 5.1a .IL spectra of implanted I301 at fluence of $4x10^{14}$ ions/cm^2.

The first 25 seconds of radiation are presented in figure 5.1b (II). The main peaks at 1.9, 2.2, 2,7 and 3.1 eV and the resultant Gaussian fitting of the IL spectrum is presented in this figure. As is clear from the figure the line at 3.1 eV vanishes to give pass to a well defined 2.7 eV band. Thus the total spectrum can be considered as the sum of the 3 leftover lines.

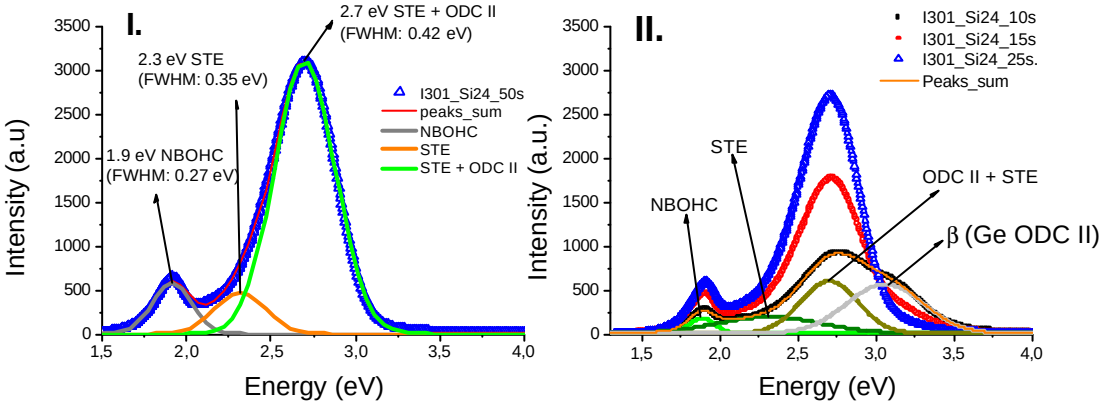

Figure 5.1b. I) Main three peaks with their respective full width at half maximum (FWHM) for the 50 s spectrum of implanted I301. II) peaks at 10 seconds.

According to A. Anneda et al. (Ref. [37]) the band at approx. 3.1 eV on figure 5.1b (II) is a superimposition of two subbands called ß, one at 3.04 eV ($ß_1$) and 3.20 eV ($ß_2$), where the difference of these bands is given by slightly different environments surrounding the active center or an intrinsic splitting of the excited state (Refs. [38,37]). The origin of this center is attributed to some non characteristic impurities of the natural silica as Ge, but oxygen deficient center might explain the origin of this beta band. As the time passes this band 3.1 eV disappears. Practically this initial 3.1 eV band is not present after the 15 seconds of irradiation.

Silicon implanted KS4V.

The main difference with respect the I301 implanted with Si is that the there is no formation of the early band at 3.1 eV. This is simply explained because the KS4V is a very pure silica, thus the possible defects created by impurities are not present. Again the behaviour with time is the same as in the I301, there is a maximum at 50 s and then the ion luminescence decreases for further time reaching a quasi stable state, as is plotted figure 5.1c. Also at 300 s the luminescence yield is less intense that the one at 15 s, which is not happening in the I301 case.

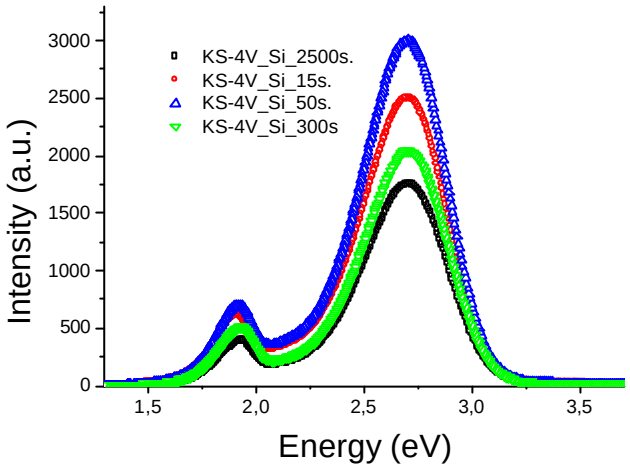

Figure 5.1c. IL spectra of implanted KS4V at fluence of $4x10^{14}$ ions/cm^2.

Silicon implanted KU1.

It is important to recall that this silica type is rich in hydroxyl molecules. It is clear in figure 5.1d (I) that again there is maximum in the 2,7 eV peak for the recollection time of 50 s of irradiation. The Gaussian fit made for the highest intensity spectrum (50 seconds) shown in figure 5.1d (II) gives practically the same values of the peaks positions and FWHM compared to the analysis made for the I301 at its maximum spectra. This similarity in the values of the bands indicates that the same defects structures are present in the different silica types.

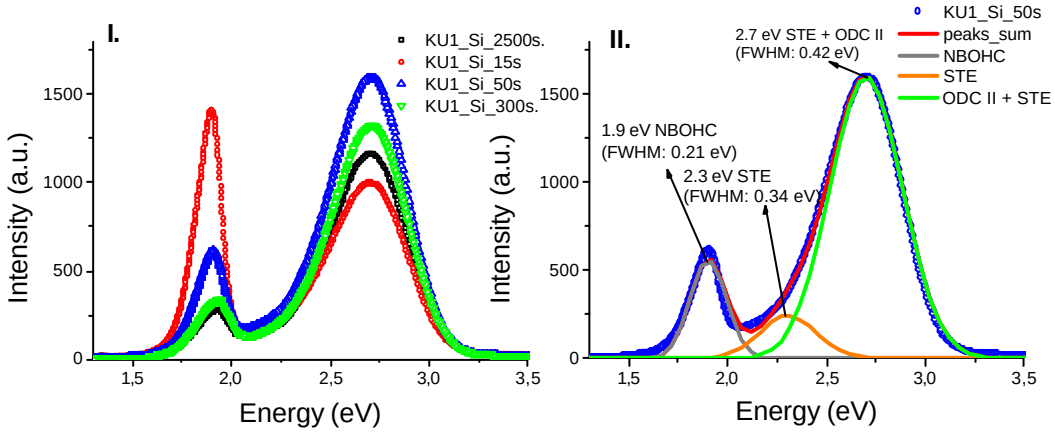

Figure 5.1d. I) IL spectra of implanted KU1 at fluence of $4x10^{14}$ ions/cm^2. II) Main three peaks of the spectrum at 50 s.

For this sample the spectrum measured at the beginning gives an intense line about 1,9 eV as it is seen in figure 5.1e, this early band eventually disappear as irradiation advance. The peak at 1,9 eV is attributed to NHBOC centers (Ref. [36]). This intense emission at 1.9 eV is related to the rupture of the OH molecule (NBOHC are created from Si-OH bonds). The band at 2,7 eV become dominant after approx. 20 seconds of irradiation. The band at 2,7 eV has a characteristic blue light while the peak at 1,9 eV gives red light (Ref. [23]), this last luminescence corresponds with excitation of the absorption bands at 4.8 and 1.97 eV (Ref. [6]). The inserted photographs in the in figure 5.1e show the corresponding light emitted by the main two bands and the superposition or combination of their light (the middle picture).

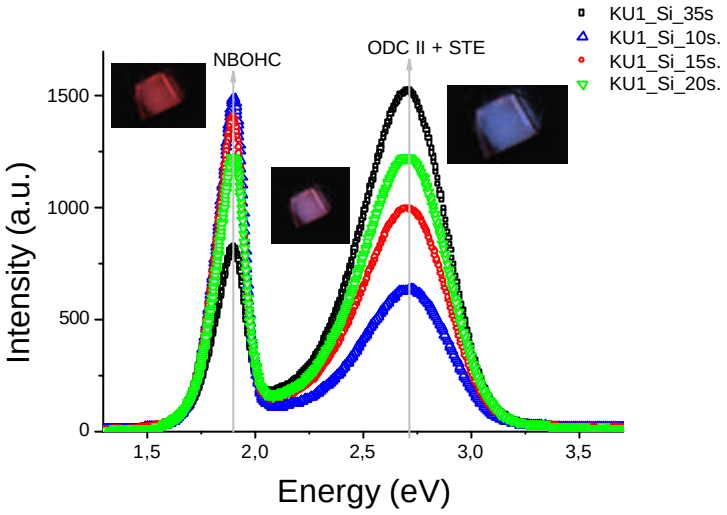

Figure 5.1e. IL spectra of implanted KU1. The pictures show the light emitted by the main two defects under radiation.

A comparison of the IL spectra for the three silica types at two different times is made in figure 5.1f. At 15 s the intensity is lower than at 50 s for all silica types. The plot at 50 s shows how the less pure silica (I301) has the higher intensity (slightly above the KS4V) of luminescence. For all the silica types as the fluence or dose increases the light yield increases up to certain maximum and then decreases reaching a saturation state (Ref. [24]). Although the KU1 silica is relatively rich in OH, its intensity was the lowest. This could be due to the fact that Si-OH bonds reduce the network strain (Ref. [2]). Strained bonds are precursors for creation of defects. Adding of interstitial H_2 helps to suppress the creation of dangling bonds (the majority of defects), at the price of generation of oxygen vacancies (Ref. [2]).

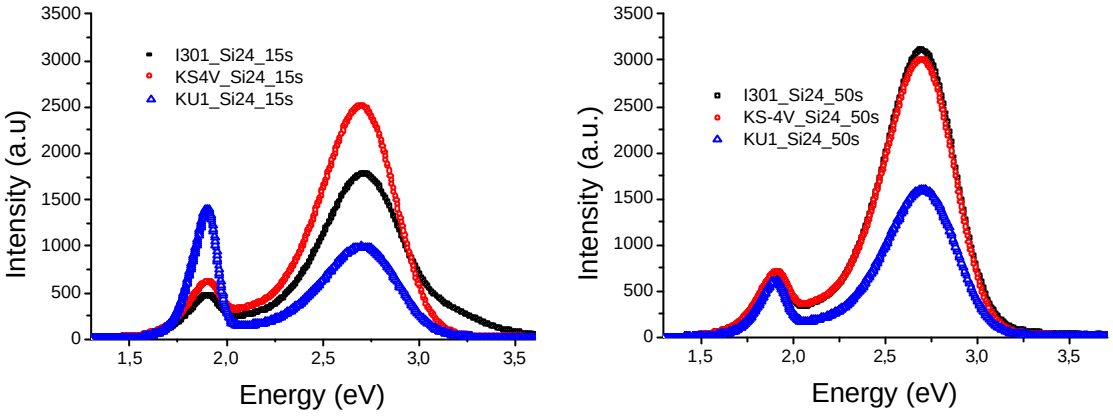

Figure 5.1f. IL spectra for the different Si implanted silicas.

A plot for the evolution with fluence (in time) of the IL main peaks is presented in figure 5.1g. The shape of the curves is very similar. The only distinctive behaviour is seen in the 1,9 eV peak intensity for KU1. This is the only intensity that actually goes lower than the intensity at 10 seconds for the first 150 seconds. Except for this case, a logarithmic increment is observed until certain time and afterwards the curve decays smoothly.

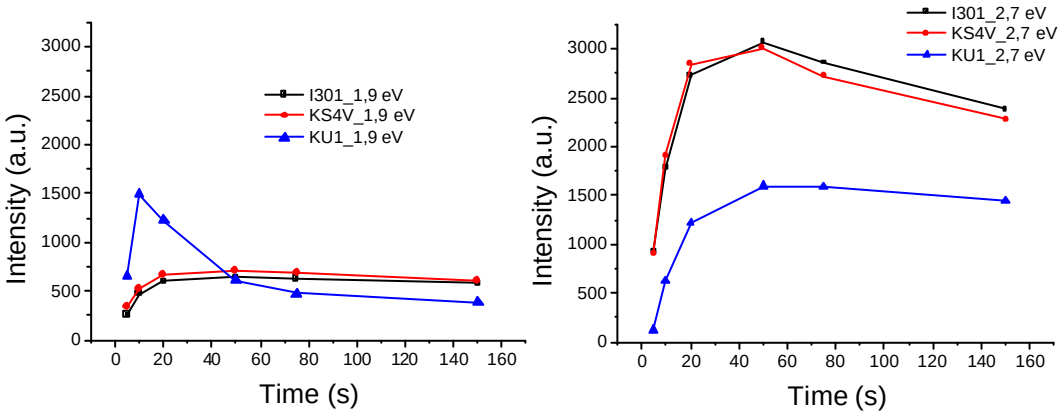

Figure 5.1g. Time evolution for 1.9 eV and 2.7 eV bands for three silica types.

In a proton beam irradiation of Si implanted silica the blue luminescence at 460 nm (2.7 eV) was attributed to ODC II. This latter band is exited by hydrogen ion bombardment (Ref. [50]).

As the time pass the luminescence intensity of the STE is reduced for all the silica types, suggesting that the induced radiation damage is acting as non radiative recombination centres (Ref. [39]). Similarly Constantini et al. (in a swift heavy ions irradiation on alpha quartz experiment) concluded that the luminescence intensity of the STE band at 2.7 eV decays due to the interaction of the STE during its radiative lifetime with the amorphous tracks which enhance non radiative recombinations (Ref. [40]). Furthermore, on a experiment of proton

irradiation on silica implanted with Si nanocrystals was found a decay in the IL emission as fluence was increased, suggesting that the damage induced by the incident protons generates non radiative centers which can inhibit the IL spectrum (Refs. [23, 24]).

5.1.2 Ionoluminescence during O implantation in I301, KS4V and KU1.

Oxygen implanted I301.

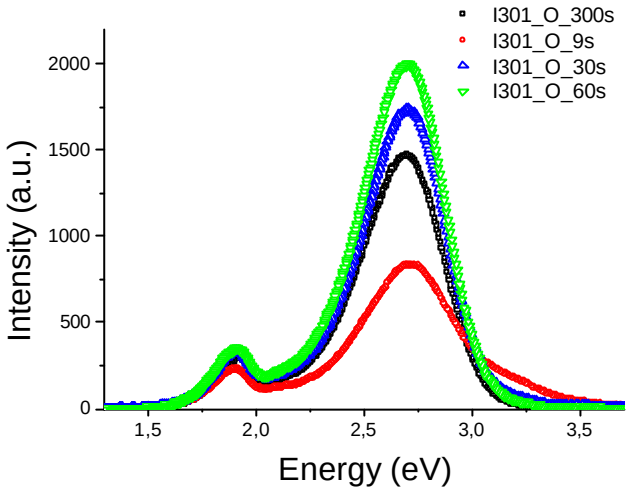

Figure 5.1h. IL spectra of implanted I301 at fluence of $6x10^{13}$ ions/cm^2.

In the case of silica implanted with oxygen the behaviour and the shape of the IL spectra is similar to the ionoluminescence spectrum of Si implanted silica, although in this case the intensity is lower compared to the I301 implanted with silicon. In the figure 5.1h the higher band is again seen at 2.7 eV and it reach it maximum at 60 seconds of irradiation.

It is noticed how the 3,1 eV band is present in this case too, although it may be possible that in this case the ODC defects are in a lower proportion as the implantation was made with oxygen, reducing maybe in a considerable way the number of oxygen vacancies. As in the silicon implanted case this band disappears with implantation fluence.

Oxygen implanted KS4V.

For this silica type the behaviour is the practically the same as in the latter case, yet there is a lower intensity. Furthermore there are no additional bands as in the I301 case at the beginning. The zoom in figure 5.1i for the 1,9 eV band shows that they relative intensity for each time has the same proportionality of the bands of the 2.7 eV.

The highest intensity for the 2.7 eV defect is reach at 60 seconds, which is happens also for the I301. The spectrum shown for 300 s is practically the same that the one for 9 s, and actually the spectrum about 400 s has lower intensity that the one for the 9s. Then in the oxygen implanted case the intensity decreases

faster that in the silicon implantation case. It should be noticed that in all figures of O and Si implantation that although the amplitude for the different defects changes, the width of each kind of peak (for each silica type) is the same.

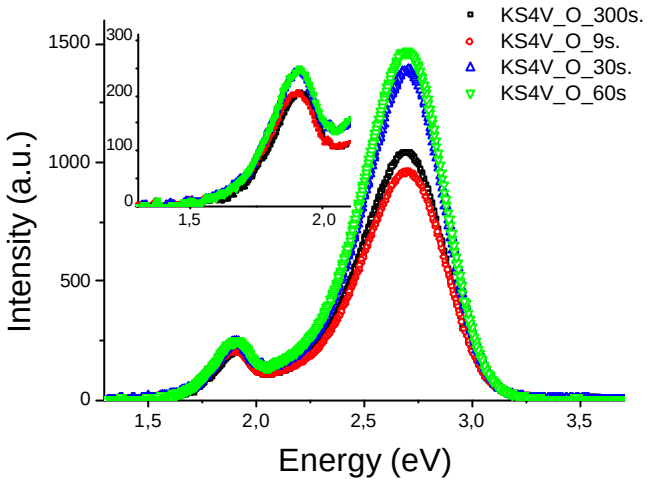

Figure 5.1i. IL spectra of implanted KS4V at fluence of $6x10^{13}$ ions/cm^2.

Oxygen implanted KU1.

Is this case as the time advances there are two main large bands produced. The one at 1,9 eV comes at the starting of the irradiation and it is predominant in the first 20 seconds. After that time the yield tends to become as the other types of silica. The maximum for the 2.7 eV band line is found to be again at 60 seconds. As the time pass up to the 10 minutes of radiation there is saturation in the light yield (Refs. [39, 41]).

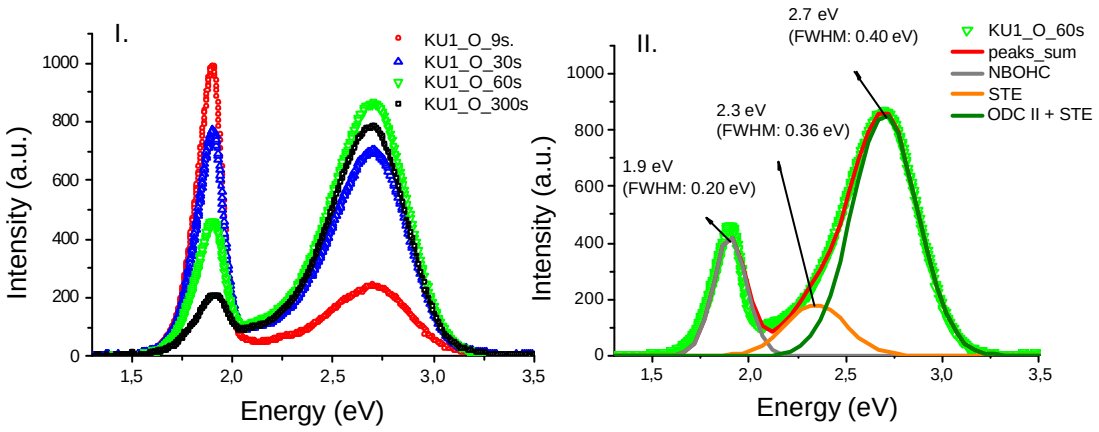

Figure 5.1j. I) IL spectra of implanted KU1 at fluence of $6x10^{13}$ ions/cm^2.
II) Peaks at 60 s. seconds.

The values of the peaks position and the FWHM obtained for the Gaussian fitting (in figure 5.1j II) of the highest spectrum were practically the same, compared to the values of the silicon implantation case. This shows once more the regularity of the characteristics of the defects.

In figure 5.1k a comparison of time evolution for the main peaks of the three samples is shown. The higher intensity for the 2,7 eV band occurred about 60 s

for the 3 different samples. Among the three types of silica the I301 silica has the higher 2,7 eV band intensity in its yields, which in turn has lower intensity compared to I301 silica implanted with silicon. The lower 2,7 eV band intensity corresponds to the KU1 silica, which has the higher intensity for the 1,9 eV band at 60 s.

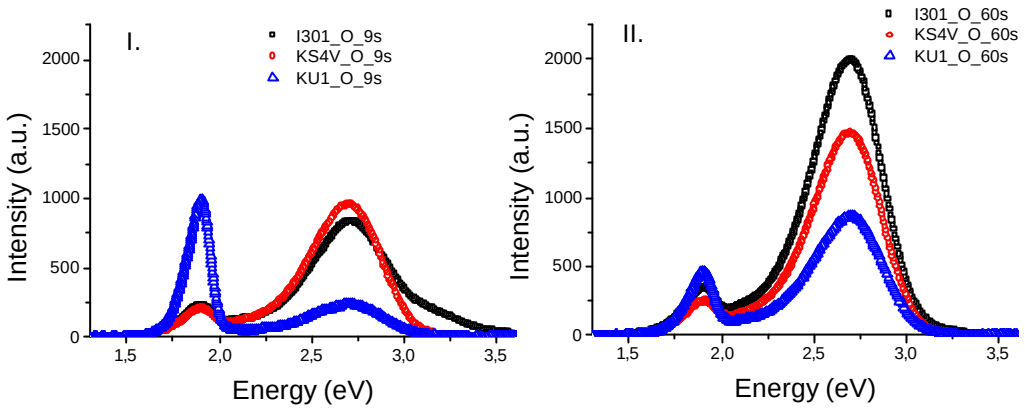

Figure 5.1k. IL spectra comparison at two times for the three silica types.

Figure 5.1l presents a time evolution comparison in the case if O implantation. The plots present the same tendency that in the case of the Si implantation.

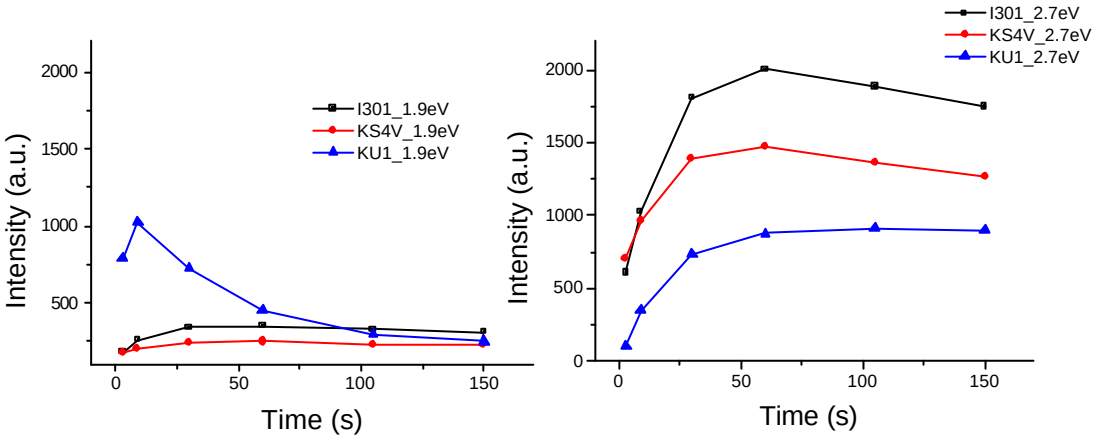

Figure 5.1l. Time evolution for 1.9 eV and 2.7 eV bands.

5.1.3 Spectra comparison for Si and O implanted samples.

As a summary the table B is presented with the parameters of the peaks founded in the above analysis. This table contains average values considering the three silica types studied in this work.

Name	Position (eV)	FWHM (eV)
NBOHC	1.9	0.20
STE	2.3	0.35
	2.7	0.40
ODC II	2.7	0.40
ß (or GeODC)	3.1	0.50

Table B. Summary of the IL peaks.

It is evident from figure 5.1m how the Si implanted silica gives higher luminescence intensity for all silica types compared to oxygen implanted case. It should be noticed that in the Si implantation was used a higher energy, thus the related fluence can produce more damage in the sample. Then higher implantation energy could be related to higher luminescence (Ref. [35]), that is, more energetic ions can penetrate the sample increasing the interaction probability leading to a more creation of defects. The bands at 2.7 eV in both cases for the KU1 are the lowest, as before; there is a decrease in intensity due to the weakening of the bonds in the presence of the OH molecule. In previous radio luminescence experimentation (with electron irradiation) was found always a far more intense spectrum in the KS4V silica that in KU1 (Ref. [39]), which is agreement with our results. The difference in intensity for the STE band can be attributed to the difference in content of OH, because the OH defects may act as non radiative recombination (radiative recombination is the photon emission coming from the binding process of an electron and an ion changing the estate of the latter) centres reducing the emission of STE and favouring phonon (phonon is a quasi particle that represents an exited state of a quantum mode of vibration of elastic structures of interacting particles) production at OH sites (Ref. [39]).

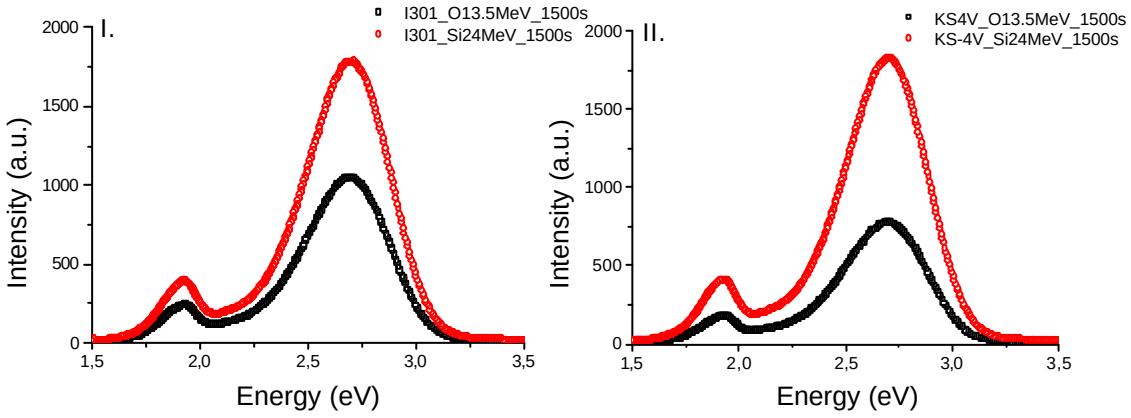

Figure 5.1m. I) IL spectra comparison for I301. II) IL spectra comparison for KS4V.

Regarding the spectra intensities, while for I301 and KS4V the IL spectrum for the silicon implantation reaches 2000 a.u., in the KU1 the intensity is under 1500 a.u. Thus if it is required low luminescence response the KU1 could be an optimal material.

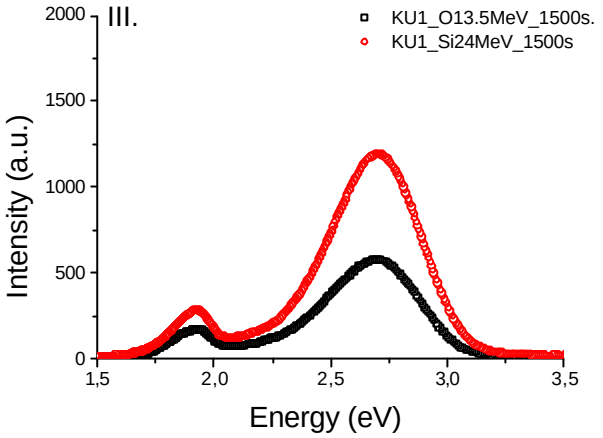

Figure 5.1m. III) IL spectra comparison for KU1.

5.2 Optical absorption results.

An analysis of the resulting absorption spectra (ranging from VUV to NIR) for the different types of silica at different implantation doses was made. Also was made a comparison of the optical absorption intensity measured in two different dates for the silicon implanted samples. This time difference was of approximately ten months. The doses of implantation were $5x10^{13}$ and $8x10^{14}$ and $1.6x10^{15}$ ion/cm^2 with silicon ion energy of 24.3 MeV and $5x10^{12}$, $1x10^{13}$, $5x10^{14}$, $1.6x10^{15}$ions/cm^2 for oxygen implantation, with oxygen ion energy of 13.5 MeV. The silica samples were implanted in the CMAM (Centro de Micro-Análisis de Materiales) from Universidad Autónoma de Madrid. All measurements were made at room temperature.

The main bands of the absorption spectra according to some authors are presented in table C.

Defects	eV Position (FHWM) Present work	eV Position (FHWM) Skuja et al [42]	eV Position (FHWM) Cannas et al [43]	eV Position (FHWM) Kajihara et al [44]	eV Position (FWHM) Magruder et al.
POL					4,8 [10]
NBOHC	4,9 very week	4,8 (1,05)			4,8-4,9 [46]
ODC(II)	5,0 (0,70)	5,03 (0,4)			5,8-5,9 [47]
POR		5,3-5,4 (1,2-1,3) week			4,8 [10]
E´	5,8 (0,80)	5,8 (0,6-0,8)			5,83 [48]
NBOHC	6,6 (0,90)	6,7-6,8 (1,7) [45]	6,4(1,7)		
NBOHC	7,3-7,4 (0,90)	7,29 (1,439)			
SiOH		7,4 [2]			
ODC(I)	7,7 (0,70)	7,6 (0,6)		7,6(0,7)	
					7,85-7,95 (Si atomic configuration related) [49]
Band-gap	8,1				

Table C. Main OA bands.

The absorption spectrum can be analyzed as sum of Gaussian bands or peaks. For the different samples and different implantation doses was found that there are essentially the same absorption bands. The intensity for the bands can vary from one sample to another. In particular, for the KS4V, KU1 and I301 silica the same bands are present, a slightly higher intensity in the bands for the I301 sample is found to be the main difference. As illustrative examples the Gaussian peaks and it resultant adjusted curve is shown for the Si and O implanted I301 spectra. It will be seen that for the other two silicas their basic spectra shapes do not change respect the I301 spectrum, and thus it not necessary to show a peaks analysis for them.

Before the implantation the optical absorption of the samples as they were received was measured. As is seen later in this work the OA of the non implanted samples is (as expected) lower in intensity than the implanted ones. In figure 5.2a

is clear how the strong bands for the I301 start appearing about 7 eV. Between 4 and 7 eV only the I301 shows well defined Gaussians bands, for which the peak about 5.1 eV is produced by Ge impurities. The bands for the KS4V are equivalent to those of the I301 but they are less intense. There is difference for the KU1 spectrum, related to the high content of OH that inhibit the appearance of the 7.6 eV band.

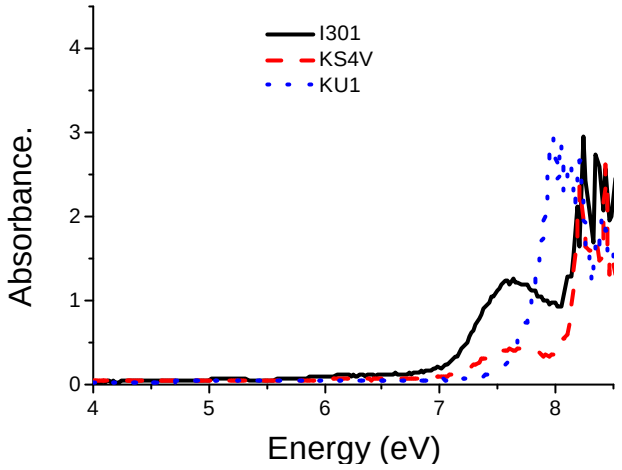

Figure 5.2a. OA of I301, KS4V, KU1 as they were received (non implanted).

5.2.1 Optical absorption after O implantation in I301, KS4V and KU1.

Oxygen implanted I301.

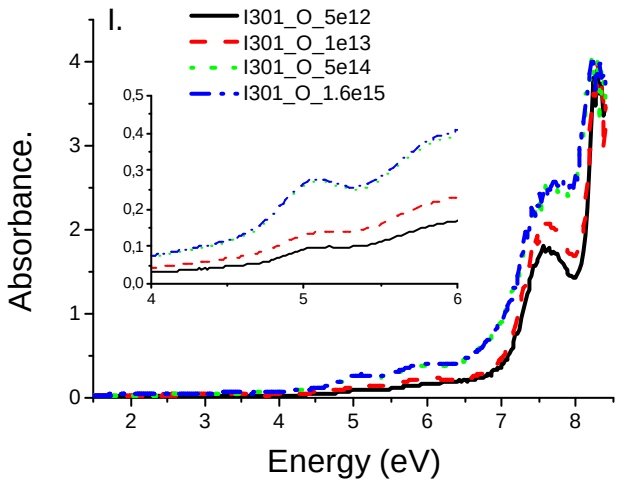

Figure 5.2b. I) OA spectra of implanted I301 at four fluencies in ions/cm2.

In figure 5.2b I it is seen how after implantation the intensity for all bands increased. There is a considerable difference between the doses of 5e14, 1.6e15 ions/cm2 and 5e12, 1e13 ions/cm2. Practically there is no difference for the OA spectra between the two highest doses, which may be interpreted as a sort of

saturation in the optical absorption, i.e. after certain fluence the OA in the material does not increase. Also the band around 5 eV corresponding to ODC II is more prominent for the two highest fluences. Analogously the band about 7.6 eV corresponding to NBOHC is observed to be higher for the two highest fluences. Figure 5.2b II shows the peaks composing the spectrum of the I301 at fluence of 1.6x1015 ions/cm2. This peaks position values are very similar to the values given by Skuja on the table C. Band around 8.2 corresponds to the band gap.

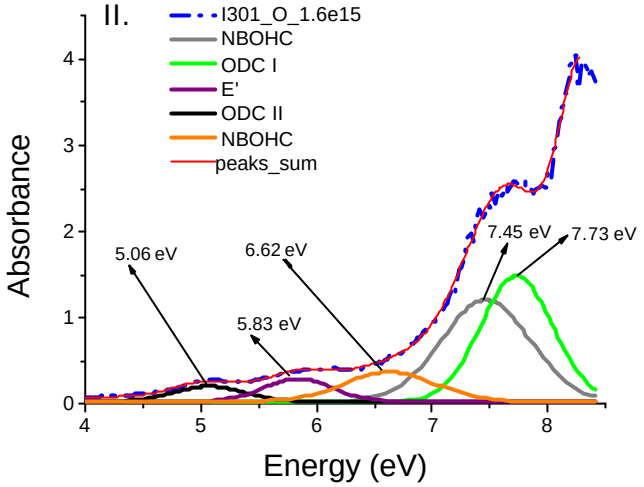

Figure 5.2b. II) Peak analysis of O implanted I301 spectrum at fluence of $1.6x10^{15}$ ions/cm^2.

Figure 5.2b III presents the same the spectrum of figure 5.2b II but with the "as received" absorbance of the I301 subtracted (note the smaller intensity in figure 5.2b III). It is notable how these two spectra are composed by the same peaks, the only difference is the peak at 4.89 eV, but its contribution to absorbance is negligible.

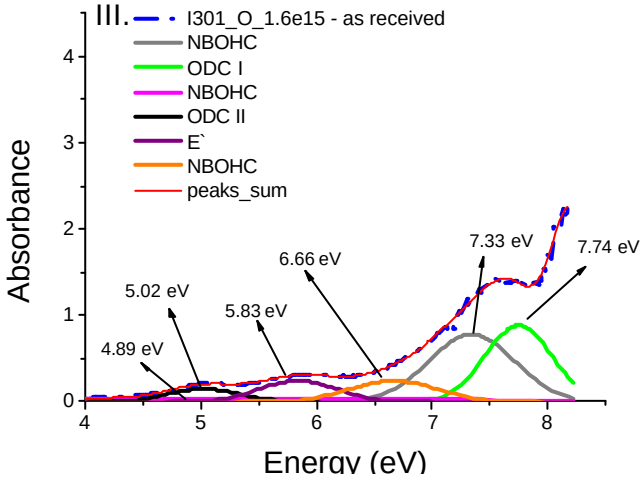

Figure 5.2b III) Peak analysis of O implanted I301 spectrum at fluence of $1.6x10^{15}$ ions/cm^2 with as received absorbance subtracted.

Oxygen implanted KS4V.

In general is observed the same absorption bands produced by the different fluences. The two higher intensities correspond to the two higher fluencies. There is no intensity difference for the two higher fluencies. The peaks about 7.7 eV are weaker with respect to the corresponding I301 silica peaks.

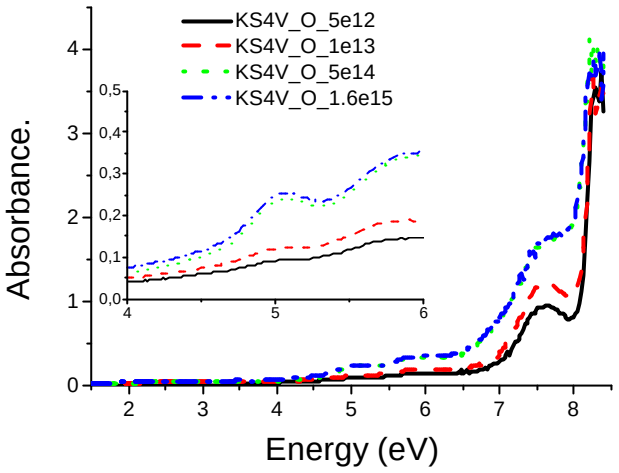

Figure 5.2c. OA spectra of implanted KS4V at four fluencies in ions/cm^2.

Oxygen implanted KU1.

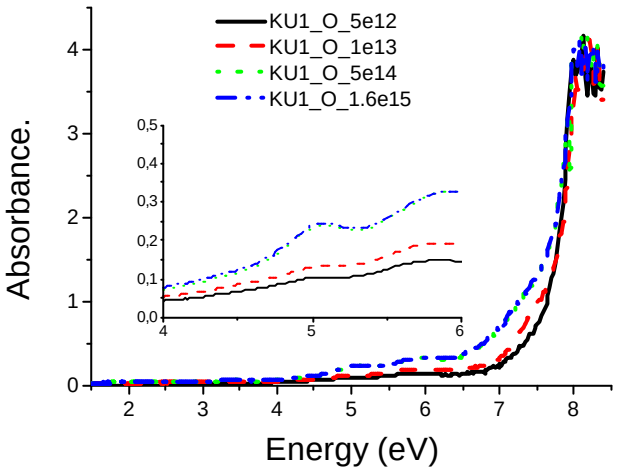

Figure 5.2d. OA spectra of implanted KU1 at four fluencies in ions/cm2.

From figure 5.2d can be seen that the band about 7.3 eV unlike the I301 and KS4V is not present for the KU1 silica.

A comparison of the three oxygen implanted silica shows the small predominance of I301 over the other two silicas in the most of the range from 1 to 7.5 eV. The band around 7.6 eV (ODC I) is not present (or is too small) in the KU1 spectrum, this is due to the effect of OH groups at high concentration, diminishing the production of this ODC. Absorption band at 7.4 eV is related to SiOH groups, it apparently has the same intensity in the three silicas.

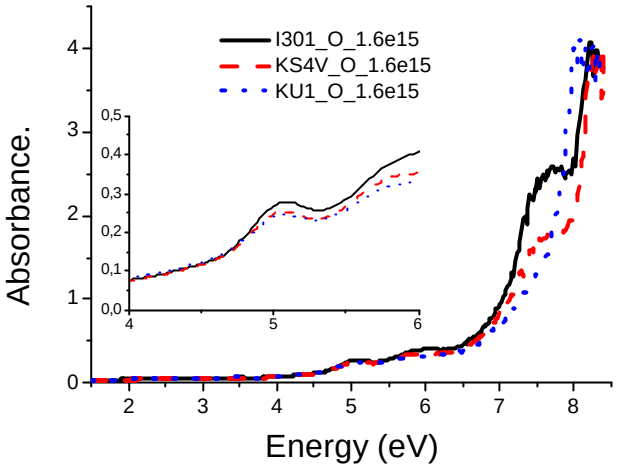

Figure 5.2e. OA comparison of the three oxygen implanted silica for a fluence of 1.6e15 ions/cm^2.

5.2.2 Optical absorption after Si implantation in I301, KS4V and KU1.

Silicon implanted I301.

As is seen in Figure 5.2f I, there is practically no difference regarding the different implantation doses, this is the absorbance at 8x10^{14} ions/cm^2 is practically the same at 5x10^{13} ions/cm^2. Measurements ten months after the implantation show a slight OA decrease (this difference does not fall into the data uncertainty), which can be due to recombination at room temperature of some defects (annealing at room temperature).

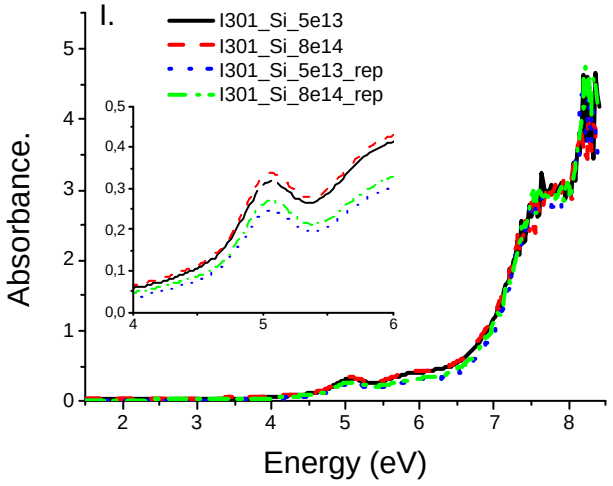

Figure 5.2f. I) Absorption spectrum of the silicon implanted I301 at two doses of implantation. 5e13 and 8e14 ions/cm^2. *rep* stands for repeated; i.e. optical absorption measurement of the same sample after 10 months.

Figure 5.2f II show the fitting peaks of the 8e14 curve, the peaks positions and their respective producing defect are indicated. According to Skuja (Ref. [2]) the region between 6 and 8 eV is difficult to adjust could be adjusted with 5 Gaussian peaks.

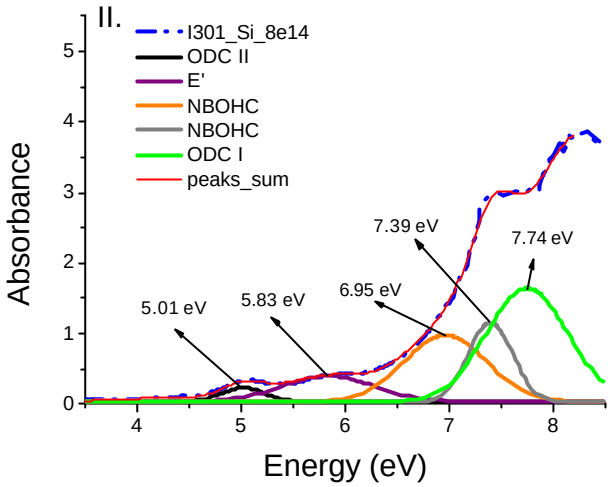

Figure 5.2f. II) Peaks analysis for I301 at $8x10^{14}$ ions/cm2.

Silicon implanted KS4V.

The order of magnitude between the spectrum curves (regarding different implantation dose) for the first measures is maintained in the second measure, the difference between them is the same difference of the last case. According to the figure 5.2f the difference for the E´ band (at the two different times) is approximately 0.04 (optical absorption dimensionless units) in the sample implanted at $8x10^{14}$ ions/cm^2. The spectra for the two different implantations for the last samples measured were practically the same. There is a change of the spectrometer devices used for the different ranges of the spectrum.

The spectrum intensity in all bands for this kind of silica is lower compared to the I301 case, which again puts in evidence the how the absorption intensity is increased depending on the quantity of impurities present in the material.

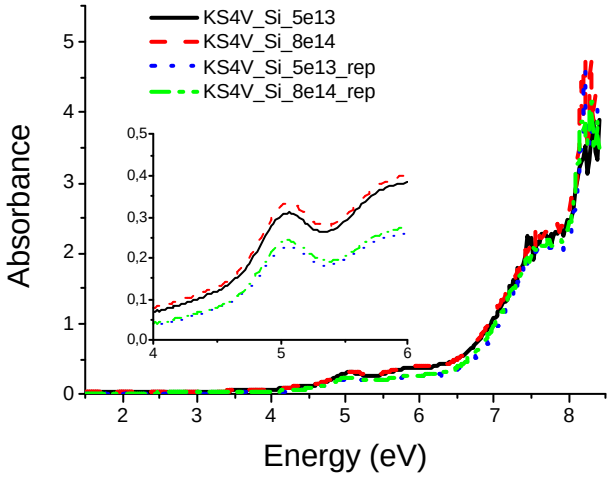

Figure 5.2g. Absorption spectrum of the silicon implanted KS4V at two doses of implantation. 5e13 and 8e14 ions/cm^2. *rep* stands for repeated; i.e. optical absorption measurement of the same sample after 10 months.

Silicon implanted KU1.

Again the intensity decay in the absorption spectrum is maintained, the most recently measured samples show lower absorption. In this case the maximum values for the E' band in the samples at dose of $8x10^{14}$ ions/cm^2 had a difference of 0.08 a.u. The inset in figure 5.2.h shows the difference in intensity more clearly for each one of the spectra. This difference is maintained over the entire range from 1 to 8 eV. Also, the difference in the first measurement for the two doses is significantly bigger compared to the cases of I301 and KS4V. In this case the intensity for all bands reach values very similar to the KS4V case.

Also can be noticed how the spectrum for both doses of the more recently measured samples is less pronounced than for the samples measured first. Thus it can be said that the samples get anneal as the time pass reaching a point of stability in terms of absorption.

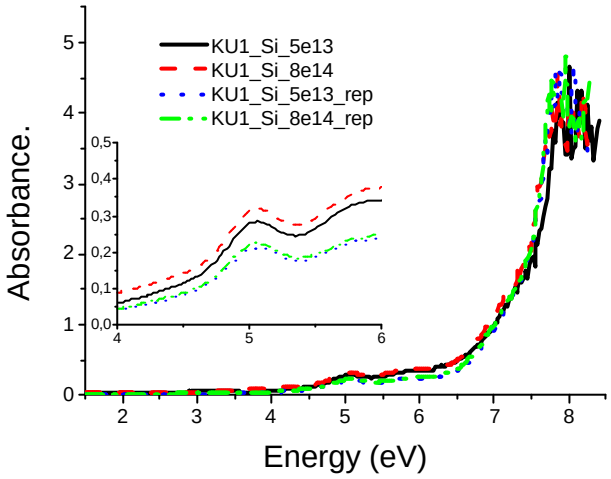

Figure 5.2h. Absorption spectrum of the silicon implanted KU1 at two doses of implantation. 5e13 and 8e14 ions/cm^2. *rep* stands for repeated; i.e. optical absorption measurement of the same samp le after 10 months.

Comparing the spectra of the three different samples is evident that the sample with more impurities (I301) has always a slightly highest intensity. This is clear in the figure 5.2i, in which the spectrum for different silica types implanted with a flux of $8x10^{14}$ ions/cm^2 (with 24.3 MeV silicon ions) is plotted.

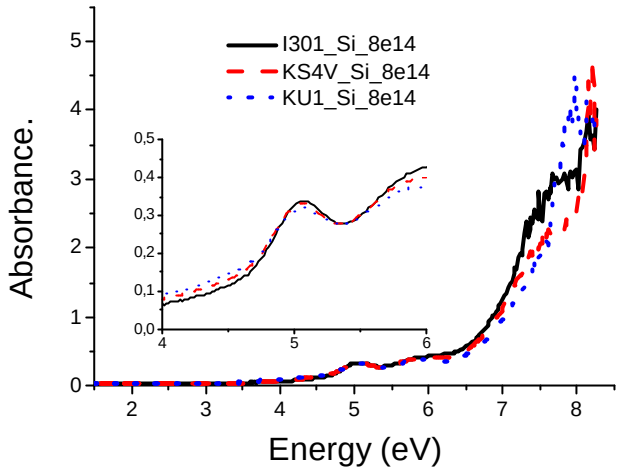

Figure 5.2i. Absorption spectra for the three silicon implanted (at 8e14 ion/cm2) silica types.

5.2.3 Spectra comparison for Si and O implanted samples.

It is important to recall that the energy for the oxygen ions in the oxygen implantation was 13.5 MeV, while this energy for the silicon ions was of 24.3 MeV. Then it should be expected more damage in the silicon implanted samples as a more energetic projectile have more probability of causing damage (assuming the same fluence for both samples). In this part the OA for the case of oxygen implanted samples and silicon implanted samples is compared for a dose of $1x10^{13}$ ions/cm^2 in both cases.

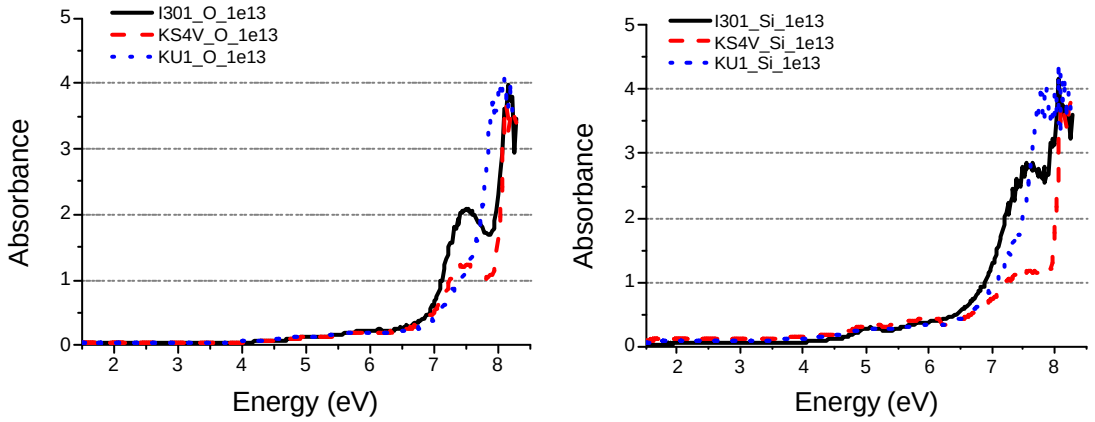

Figure 5.2j. OA of I301, KS4V and KU1 compared at a fluence of $1x10^{13}$ ions/cm^2.

From figure 5.2j is notable that about the same OA intensity in reached in both cases although the intensity (around 7.5 eV) for the I301 silica is higher for the silicon implantation case. Also is noted a displacement to the left in the band-gap band in the KU1 for the Si implantation.

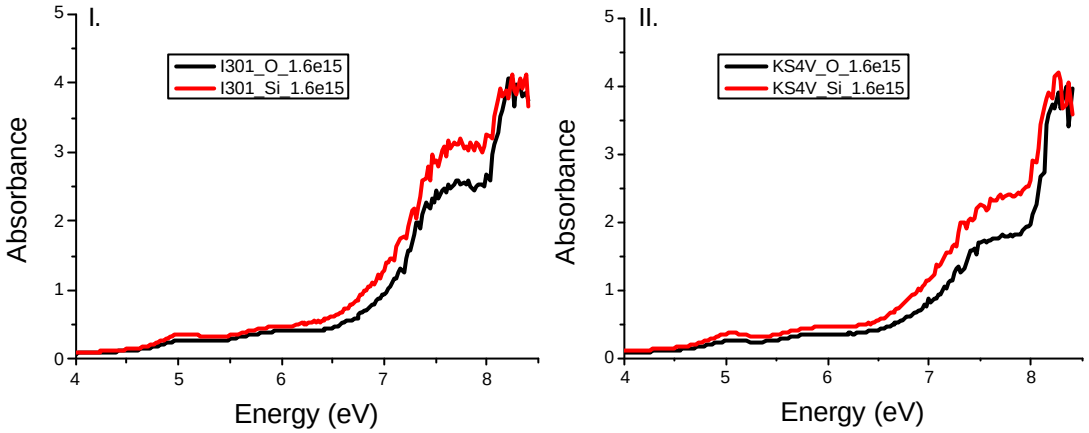

Figure 5.2k. I) I301 OA comparison for Si and O implantation. II) KS4V OA comparison for Si and O implantation. Both plots at fluence of $1.6x10^{15}$ ions/cm^2

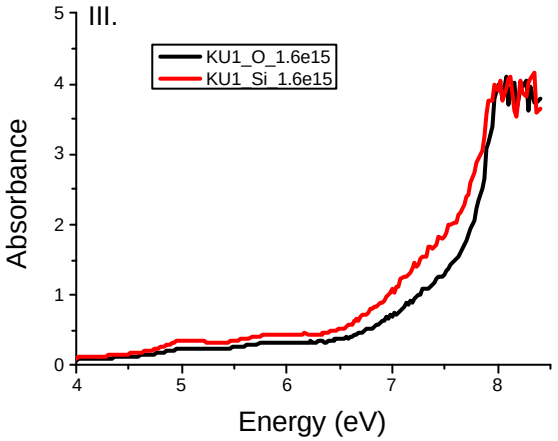

Figure 5.2k. III) KU1 OA comparison for Si and O implantation.

From figure 5.2k is possible to conclude that Si implantation produced a slightly higher absorbance in the three silica types.

Chapter 6.

Conclusions.

Implantation at several fluences of 24.3 MeV Si+4 ions and 13.5 MeV O+4 ions (with penetration of ~ 9 µm) in silica samples with different impurities and OH content was made to study the effect of self-ion implantations and correlate defect creation with fluence and local non-stoichoimetry. Two silica types used (KS4V and KU1) are reference materials in ITER to be used in optical diagnostic systems. The luminescence and optical absorption obtained for the studied silicas are directly related to the defects produced by the implantation the silica matrix.

IL measurements.
During the implantation measurements of the IL spectra for I301, KS4V and KU1 silica types has been done. In all cases were detected two main bands at 2.7 eV (blue band) associated to STE defects plus ODC II defects and 1.9 eV (red band) associated to NBOHC defects. A third band at 2.3 eV corresponding also to STE was detected in all cases too.

All the important changes in the IL spectra occurred at low fluences ($<1x10^{13}$ ions/cm^2; the first minute of the implantation). However the evolution of the different defects is different for each silica type:
In the I301 an emission band at 3.1 eV was obtained at fluences lees than $3x10^{12}$ ions/cm^2 (first 15 seconds of irradiation), which is related to Ge ODC defects. This band is not present in KU1 or KS4V. The I301 silica has the higher contents of impurities.

At low fluencies in the KU1 silica presented a relatively high intensity for the 1.9 eV peak, which is attributed to the rupture of the OH group. It can be concluded that the OH impurities in the KU1 silica increased substantially the intensity of the 1.9 eV band.

In all silicas after the maximum of IL is reached, the IL decreases to a roughly steady luminescence spectrum, it is possible to infer that creation and recombination of defects is reducing and after inhibiting the light yield.

KU1 presents the lower IL intensity, probably due to its high OH content. The OH impurity produces the relaxation of strained bonds making them more stable, this result in less production of defects in the silica network and therefore less luminescence.

OD measurements.
Optical density after implantation of I301, KS4V and KU1 silicas was studied in a wide range of wavelengths from VUV to NIR. There are five perfectly differentiated bands in all silica types, corresponding to the following defects ODC II (5 eV), E' (5.8 eV), NBOHC (6.7 and 7.4 eV) and ODC I (7.7 eV).

Optical Density (OD) intensity of Si implanted samples was higher than OD of O implanted samples in all cases.

The optical absorption spectra of Si implanted samples were measured after 10 months of the implantation and the results showed a decrease in the optical absorption (the samples are suffering an annealing process at room temperature).

The bands found in each one of the silica types at any doses were the same, the only differences was the intensity of the absorption spectrum. The impurities produce a higher creation of defects into the sample, and thus as higher the impurities content in the sample (I301 silica) higher the optical absorption.

For Si implanted samples there is just very small difference in the OA spectra measured doses from $5x10^{13}$ to $1.6x10^{15}$ ions/cm^2. There is saturation in the OA spectra at fluence of 5×10^{13} ions/cm^2.
In the case of oxygen implantation the OA saturation is reached at higer fluence (over 5×10^{14} ions/cm^2) than in Si implantation.

The creation of defect produced by implantation for the three silica types give place to the same basic absorbance, independently of OH content or impurities content.

References.

[1] G. Vayakis, E.R. Hodgson, V. Voitsenya, C.I. Walker. Fusion Science and Technology 53, 699 (2008).

[2] L. Skuja, M. Mirano, H. Hosono, and K. Kajihara, Phys. Status Solidi. C2 No 1, 15 (2005).

[3] G. Pachioni, L. Skuja, D.L. Griscom (eds.) *Defects in SiO2 and related dielectrics: Science and technology* (Kluver Academic Publichers, 2000).

[4] N. Wiberg, A. Holleman, E. Wiberg. *Inorganic Chemistry* (Academic Press, 1st edition, London, 2001)

[5] L. Hobss, X. Yuan. *Defects and disorders in crystilline and amorphous solids* (Kluwer Academic Publisher, Dordecht, 2000).

[6] Salh, Roushdey. Defect related luminescence in silicon dioxide network: a review. *Crystalline Silicon-Properties and uses* (Sukumar Basu (ed) 135, 2011).

[7] G. Heterington, K. Jack, M. Ramsay. Phys. Chem. Glasses 6, 6 (1965).

[8] M. León Pichel, Doctoral thesis: *Efectos de la radiación gamma y neutrónica en las propiedades ópticas del oxido de silicio amorfo*, Universidad Autónoma de Madrid, (2011).

[9] R. Magruder III, R Weeks, R.Weller, J. of Non-crystaline Solids 357, 1615 (2011).

[10] R. Magruder III, R Weeks, R.Weller, R. Zuhr, J. of Non-crystaline Solids 304, 224 (2002).

[11]K. Moritani, Y. Teraoka, I. Takagi, H. Moriyama. J. of Nuclear Materials 329, 988 (2004).

[12] L. Skuja, J. of Non-crystaline Solids 239, 16 (1998).

[13] S. Ismail-Beigi, S. Louie. Physical Review Letters 95, 1 (2005).

[14] J. Lee, M. Tomozawa, R McCrone. J. of Non-crystaline Solids 354, 1509 (2008).

[15] V. Plotnichenko, V. Sokolov, E. Dianov. J. of Non-crystaline Solids 261, 186 (2000).

[16] J. Shelby. J. Appl. Phys 50, 3072 (1979).

[17] G. Walrafen, S. Samanta. J. Chem. Phys. 69, 493 (1978)

[18] H. Bach, N. Neuroth, *The Properties of Optical Glass* (Springer, Berlin Heidelberg, 1995).

[19] R.J. Reynolds, K. Aldous, *Atomic Absorption Spectroscopy* (Charles Griffin and Company, London, 1970).

[20] J. Walker. Rep. Prog. Phys. 42, 1606 (1979).

[21] I.I. Sobelman, *Introduction to the theory of atomic spectra* (Pergamon Press, Oxford, 1 edition 1972).

[22] J. Markham. Rev. Mod. Phys. 31, 956 (1959).

[23] D. Jimenez-Rey, O. Peña-Rodríguez, J. Manzano-Santamaría, J. Olivares, A. Muñoz-Martin, A. Rivera, F. Agulló-López, Nuclear Instruments and Methods in Physics Research. B (2012) (doi: 10.1016/j.nimb.2011.12.025).

[24] J. Demarche, D. Barba, G. Ross, G. Terwagne. Nuclear Instruments and Methods in Physics Research B (2012) (doi: 10.1016/j.nimb.2011.01.051).

[25] P. Townsend. Rep. Prog. Phys. 50. 501 (1987).

[26] S.I. Kononenko, O.V. Kalantaryan, V.I. Muratov, V.P. Zhurenko. Radiation Mesurements 42, 751 (2007).

[27] A. Morono, E.R. Hodgson, , S. M. González de Vicente, Journal of Nuclear Materials,1002, 386 (2009).

[28] G.E. King, A.A Finch, R.A. Robinson, D.E. Hole. Radiation Measurements 46, 1 (2011).

[29] A. Bettiol, K. Nugent, D. Jamieson. Nuclear instruments and methods in Physics Research B 130, 734 (1997).

[30] F. Mota et al. Journal of Nuclear Materials 329-333, 1190 (2004).

[31] F. Mota et al. Fusion Engineering and Design 75-79, 1027 (2005).

[32] J. Mahan, A. Vantomme. J. Vac. Sci. Technol. 15(4), 1976 (1997).

[33] B. Brichard, A. Tomashuk, B. Bogatyrjov, A. Fernandez. Journal of non crystalline solids 353, 466 (2007).

[34] Heraeus Quarzglas, Chemical Purity, *http://heraeus-quarzglas.com/en/quarzglas/chemicalpurity/Chemical_purity.aspx,* 2012.

[35] K Moritani, J. Takemoto, I. Takagi, M. Akiyoshi, H. Moriyama. Journal of Nuclear Materials 384, 19 (2009).

[36] O. Peña-Rodríguez, D. Jimenez-Rey, , J. Manzano-Santamaría, J. Olivares, A. Muñoz-Martin, A. Rivera, F. Agulló-López, Applied Physics Express 5, 011101 (2012).

[37] A. Anedda, R.Boscaino, M. Cannas, R. Corpino, F. Gelardi, M. Leone. Nuclear Instruments and methods in Physics Research B 116, 360 (1996).

[38] S. Agnello, R.Boscaino, M. Cannas, F. Gelardi, M. Leone. Physical Review B. 61, No. 3 (2000).

[39] A. Moroño, E. Hodgson. Journal of Nuclear Materials, 367-370, 1107 (2007).

[40] J. Constantini, F. Brisard, G. Biotteau, E Balanzat, B. Gervais. Journal of Applied Physics 88 No 3, 1339 (2000).

[41] S. Nagata, S. Yamamoto, A Inouye, B. Tsuchiya, K. Toh, T. Shikama. Journal of Nuclear Materials 367-370, 1009 (2007).

[42] L. Skuja, K. Kajihara, M. Hirano, and H: Hosono, Physical Review B 84, 205206 (2011).

[43] M. Cannas , F.M. Gelardi Phys Rev B, 69 (2004) 153201

[44] K. Kajihara et al. Journal of Non-Crystalline Solids 354, 224 (2008)

[45] H. Hosono, K. Kajihara, T. Suzuki, Y. Ikuta, L. Skuja, and M.Hirano, Solid State Commun 122, 117 (2002).

[46] R. Magruder III, A. Stesmans, K Clémer, R Weeks, R.Weller, J. of Non-crystaline Solids 352, 3027 (2006).

[47] R. Magruder III, A. Stesmans, K Clémer, R Weeks, R.Weller, J. of Applied Physics 100, 033517 (2006).

[48] R. Weeks, R Magruder III, A. Stesmans, J. of Non-crystalline Solids. 354, 208 (2008).

[49] R. Magruder, R. Weeks, Y. Morimoto, Nuclear Instruments and Methods in Physics Researh. B 269, 2532 (2011).

[50] G. Gawlik, J. Jagielski, A. Stonert, R. Ratajczak. Nuclear Instruments and Methods in Physics Research B 267, 2579 (2009).

[51] K. Michaelian, A Menchaca, S. Hilarion. J. of luminescence 72-74, 740 (1997).

Acknowledgements.

I want to thank the unconditional support of my family.

Declaration in lieu of oath

Herewith I declare in lieu of oath that I have prepared this thesis exclusively with the help of my scientific teachers and the means quoted by them.

City, the _____

Luis Alonso Araya Solano

Copyright Agreement

I hereby grant the FUSION-EP consortium the non-exclusive right to publish this work.

I declare that this work is free of copyright claims of third parties.

City, the _____

Luis Alonso Araya Solano